Chemical Geology 657 (2024) 122101

Contents lists available at ScienceDirect

Chemical Geology

journal homepage: www.elsevier.com/locate/chemgeo

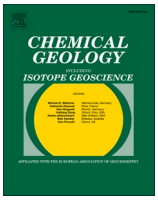

Surface water oxygenation and low bioproductivity during deposition of iron formation of the Jacadigo Group (Brazil): Insights from combined cadmium – Chromium isotopes

Robert Frei [a,*], Claudio Gaucher [b], Paulo César Boggiani [c], Jesper Allan Frederiksen [a], Samantha Renee Walker [a], Henrique Albuquerque Fernandes [c], Fabricio Caxito [d]

[a] University of Copenhagen, Department of Geosciences and Natural Resource Management, Øster Voldgade 10, Copenhagen K 1350, Denmark
[b] Instituto de Ciencias Geológicas, Facultad de Ciencias, Universidad de la República, Iguá 4225, Montevideo 11400, Uruguay
[c] Instituto de Geociências, Universidade de São Paulo, São Paulo, SP, Brazil
[d] CPMTC Research Center and Postgraduate Program in Geology, Universidade Federal de Minas Gerais, Belo Horizonte 31270–901, Brazil

ARTICLE INFO

Editor: Vasileios Mavromatis

Keywords:
Chromium isotopes
Cadmium isotopes
Banded iron formation
Bioproductivity
Ocean redox
Jacadigo Group
Brazil

ABSTRACT

The Banda Alta Formation (Urucum district, Mato Grosso do Sul, Brazil) comprises ~600 Ma Fe and Mn deposits, which are among the world's youngest and largest Neoproterozoic sedimentary Fe and Mn formations (IF; MnF). These have been deposited in a redox-stratified, marine sub-basin (Jacadigo Basin), which was strongly influenced by glacial advance/retraction cycles with temporary influx of continental freshwater and upwelling of metal-enriched deep anoxic seawater. Cr and Cd isotopes measured on meticulously separated hematite mesobands from drill core samples are relatively homogenous throughout the ca. 325 m thick sequence sampled in the Banda Alta Fm., with average authigenic δ^{53}Cr values of +0.93 ± 0.24 ‰ (2σ; n = 23) and δ^{114}Cd values of −0.14 ± 0.14 ‰ (2σ; n = 15). The significant enrichment of Cr, in parallel with the strong enrichments of other redox sensitive elements (U, Mo), attests for effective and efficient reduction removal processes in the surface waters during cycles where upwelling Fe^{2+}-rich waters reached the oxygenated surface layer exposed to the atmosphere during episodic glacier retreat stages. Assuming a similar quantitative and efficient removal pathway of dissolved Cd by iron oxyhydroxides, the so-inferred average δ^{114}Cd signature of −0.14 ± 0.14 ‰ in the Jacadigo Basin surface water is significantly lower than signatures of modern ocean surface waters with a range of δ^{114}Cd of ca. ~0.4 to ~1 ‰ and even lower than the signature of modern ocean deep waters with δ^{114}Cd of ~0.3 ‰. It possibly attests to reduced primary production levels and lower nutrient utilization rates during deposition of the Late Neoproterozoic Jacadigo Group, compared to today. This despite the inferred oxidized surface water layer that must have prevailed during this time, as implied by the strongly positively fractionated Cr isotope signatures and pronouncedly negative Ce-anomalies recorded in the seawater-like, shale-normalized Rare Earth Element and Yttrium (REY) patterns exhibited by the hematite mesobands. Data presented herein speak for: (1) a stable, isotopically heavy Cr input to the Jacadigo Basin at the time of deposition, implying high atmospheric O_2 levels in the Late Neoproterozoic (2) likely quantitative, reductive incorporation / adsorption processes of dissolved Cr and Cd, respectively, into/onto precipitating iron oxyhydroxides, and (3) the prevalence of low nutrient concentrations and utilization rates in the Jacadigo Basin during glacier retreat cycles. Banded iron formations are considered suitable archives for reconstructing redox and bioproductivity levels in past marine depositional basin, including those prevalent in Neoproterozoic glacial conditions, via employing the Cr—Cd isotope double tracer to iron-rich mesobands.

1. Introduction

After prominent deposition of Banded Iron Formations (BIF) during the Archean and early Paleoproterozoic, particularly during the Great Oxidation Event (GOE) ~ 2.47–2.19 Ga (Bekker et al., 2004; Gumsley et al., 2017; Hodgskiss and Sperling, 2021; Poulton et al., 2021), a lack

* Corresponding author.
E-mail address: robertf@ign.ku.dk (R. Frei).

https://doi.org/10.1016/j.chemgeo.2024.122101
Received 26 January 2024; Received in revised form 9 April 2024; Accepted 12 April 2024
Available online 25 April 2024

of IF deposition characterizes the late Paleoproterozoic and Mesoproterozoic between ~1.85–1.0 Ga (Eriksson et al., 2004; Yin et al., 2023, and references therein). Weak or even lack of ocean oxidation was used to explain the absence of BIF deposition in this period (Bekker et al., 2010; Holland, 1984; Slack et al., 2007). Others explained the lack of IFs as a consequence of widespread development of euxinic (anoxic and sulfidic) deep-ocean conditions along productive continental margins (Canfield et al., 2008; Poulton et al., 2010). IFs were again deposited in the Neoproterozoic on a large scale (Bekker et al., 2010; Klein, 2005). Many of these Neoproterozoic IFs were formed during global glaciation events and were associated with drastic environmental changes. The most prominent glaciation events during which IFs were deposited worldwide are the Sturtian (middle Cryogenian), Marinoan (late Cryogenian) and the Gaskiers (Ediacaran) glacial events (Halverson et al., 2010). Dissolved ferrous iron (Fe^{2+}) was able to accumulate in the anoxic bottom water layers of respective redox-stratified depositional basins. Such environmental conditions were favorably established during ice coverage in time periods where glaciers shielded the basin waters against the atmosphere (Baldwin et al., 2012). Upwelling of these Fe^{2+} fertilized bottom waters into oxygenated water layers in glacier retreat stages then enabled the oxidation of ferrous Fe (Fe^{2+}) to ferric Fe (Fe^{3+}) and the subsequent flocculation and deposition of iron oxyhydroxides as the IF precursors (Beukes and Klein, 1990; Klein and Beukes, 1993). There are also examples of some Neoproterozoic BIFs that are volcanogenic-associated, similar to the Paleo- to Neoarchean greenstone belt associated Algoma-type BIFs and some that are passive margin marine sediment-associated, similar to the Neoarchean to Paleoproterozoic Superior-type BIF (Basta et al., 2011; Bekker et al., 2010; Gaucher et al., 2015; Sial et al., 2015; Stern et al., 2013; Yu et al., 2022).

The increase of O_2 in the Neoproterozoic atmosphere (often referred to as the Neoproterozoic oxidation event (NOE), timely correlated with near-global glaciations, was ascribed to an increase of phytoplankton productivity; Frei et al., 2009). The appearance of the Ediacara fauna at ~575 Ma (Droser and Gehling, 2015; Narbonne, 2005) succeeded the NOE, and deep ocean anoxia and ferruginous conditions apparently prevailed throughout the latest Neoproterozoic and even into the Cambrian (Canfield et al., 2008; Johnston et al., 2010; Li et al., 2010).

The Fe and Mn deposits in the Urucum district pertain to the Banda Alta Formation (Jacadigo Group; Fig. 1) in Mato Grosso do Sul State, Brazil, and are associated with glaciogenic deposits. The Urucum IF is one of the NOE-related IF deposits that appears to be tightly associated to a glaciation event and therefore could be regarded as to fit depositional environments that persisted during “Snowball Earth” scenarios (Kirschvink, 1992) in which ice covers prevented exchange of oxygen between atmosphere and oceans and so enabled accumulation of dissolved Fe^{2+} in in the oceans (Beukes and Klein, 1992; Klein and Beukes, 1993). One model which describes the potential causes for the recovery from large-scale glaciation is that conveyed, among others, by Allen and Etienne (2008), Le Hir et al. (2009) and Peltier et al. (2007). These authors suggested that voluminous volcanic outgassing may have led to increased atmospheric CO_2 levels that could have reached 350 times present atmospheric levels (PAL) and so created strong greenhouse conditions (Hoffman et al., 1998). The study by Frei et al. (2017), and that recently published by Árting et al. (2023), on BIFs from Morro Urucum (M. Urucum; Fig. 1), contributed to testing this model. These two studies used the Cr isotope redox-proxy on surface and drill core samples of IFs across the Urucum ore district. Both studies assume that the mass budgets of Cr in the oceans is substantially controlled by Cr released from the continental land masses by oxidative weathering processes and that the isotope composition of dissolved Cr in at least present day ocean surface water is substantially controlled by primary productivity (Frei et al., 2014). The positively fractionated Cr isotope signatures that Árting et al. (2023) and Frei et al. (2017) measured on the Urucum IF led these authors to postulate that these signatures were likely caused by widespread oxidative release of Cr(VI) from the continents, rather than by acidic release of Cr(III) caused by elevated CO_2 greenhouse-like conditions.

However, Janssen et al. (2020), Scheiderich et al. (2015), and Semeniuk et al. (2016) proposed that the Cr isotope compositions in the photic layers of present-day oceans are likely and primarily controlled by biological productivity.

Here we present, for the first time, combined Cr - Cd stable isotopes, rare earth element and yttrium (REY) patterns, and redox sensitive trace element and selected major element data, of carefully separated hematite mesobands from IF of the Banda Alta Fm., in order to assess surface water redox conditions and bioproductivity under glacial environmental conditions during the late Neoproterozoic.

1.1. Cr and Cd cycles

The oceans receive Cr through continental run-off or hydrothermal vent fluids. Vent fluids are characterized by isotopically unfractionated Cr ($\delta^{53}Cr = -0.12 \pm 0.11$ ‰; Schoenberg et al., 2008), while continentally derived Cr, released by oxidative weathering, may be positively fractionated. Oxygen in the atmosphere is a driver for the oxidation of immobile Cr(III) in rocks and soils to soluble Cr(VI) in the presence of Mn-oxides, which act as reaction catalysts (Oze et al., 2007). The mobile Cr fractions are partially reduced again and this process is accompanied by fractionation processes which render the finally mobilized Cr(VI) positively fractionated (D'Arcy et al., 2016; Farkaš et al., 2013; Frei et al., 2009; He et al., 2020; Novak et al., 2017; Paulukat et al., 2015; Wu et al., 2017). The positively fractionated dissolved Cr(VI) compounds reach the oceans via run-off where they either are sorbed onto particles or are, either biologically (Janssen et al., 2020; Scheiderich et al., 2015; Semeniuk et al., 2016) or abiologically (Frei et al., 2009; Janssen et al., 2022), reduced to insoluble Cr(III) bearing species. These finally are then deposited in marine sediments. In essence, the input sources of Cr into the oceans are a mixture of three end members: (1) hydrothermal Cr (III), (2) unfractionated continental Cr(III) carried by suspended load or dissolved organically bound compounds, and (3) soluble and fractionated continental Cr(VI) compounds. As mentioned above, the overall dissolved Cr isotope signal may be further altered by biogenic redox processes in the water column. Such processes involve reduction by organic matter (Janssen et al., 2020; Rickli et al., 2019; Semeniuk et al., 2016), and incorporation into carbonates (Frei et al., 2011; Wei et al., 2018b) and Fe—Mn crusts (Wei et al., 2018a). Vital effects on Cr isotope compositions have also been demonstrated for carbonate-precipitating organisms such as bivalves (Bruggmann et al., 2019a; Frei et al., 2018) and for uptake of Cr by planktonic foraminifera (Wang et al., 2016). Under the assumption that dissolved Cr is predominantly composed of Cr(VI), and that there is surplus fertilization of the ocean waters with dissolved Fe^{2+}, then chemical sediments such as IFs have the potential to record the positively fractionated surface seawater $\delta^{53}Cr$ signature. However, this assumption is only valid if reductive removal of Cr by a Fe-oxyhydroxide shuttle is efficient and quantitative (Døssing et al., 2011; Frei et al., 2016; Frei et al., 2009). In such a scenario, the fate of Cr, and ultimately the Cr records in iron-rich chemical sediments, are linked to atmospheric oxygenation, intensity of release of chromium from the continents, and levels of primary productivity. Studies reporting Cr isotope signals in IFs have been used to reconstruct Earth's atmospheric oxygenation at different times in the past, and ultimately as one more tool to delineate and record climate changes in the Precambrian (Frei et al., 2016; Frei et al., 2009; Konhauser et al., 2011; Wei et al., 2018c).

Oceans receive Cd via three main sources. These are the upper continental crust ($\delta^{114}Cd = -0.01 \pm 0.04$ ‰; Rehkämper et al., 2012; Schmitt et al., 2009), rivers ($\delta^{114}Cd = 0.1$ to 0.3‰; Lambelet et al., 2013) and aerosols/dust ($\delta^{114}Cd = -0.19$ to 0.19‰; Bridgestock et al., 2017). The Cd composition of deep ocean seawater is isotopically heavier with $\delta^{114}Cd$ of 0.35 ± 0.12‰ (Conway and John, 2015a; Conway and John, 2015b; Janssen et al., 2017; John et al., 2018; Ripperger et al., 2007; Sieber et al., 2019; Xie et al., 2017). Light cadmium isotope

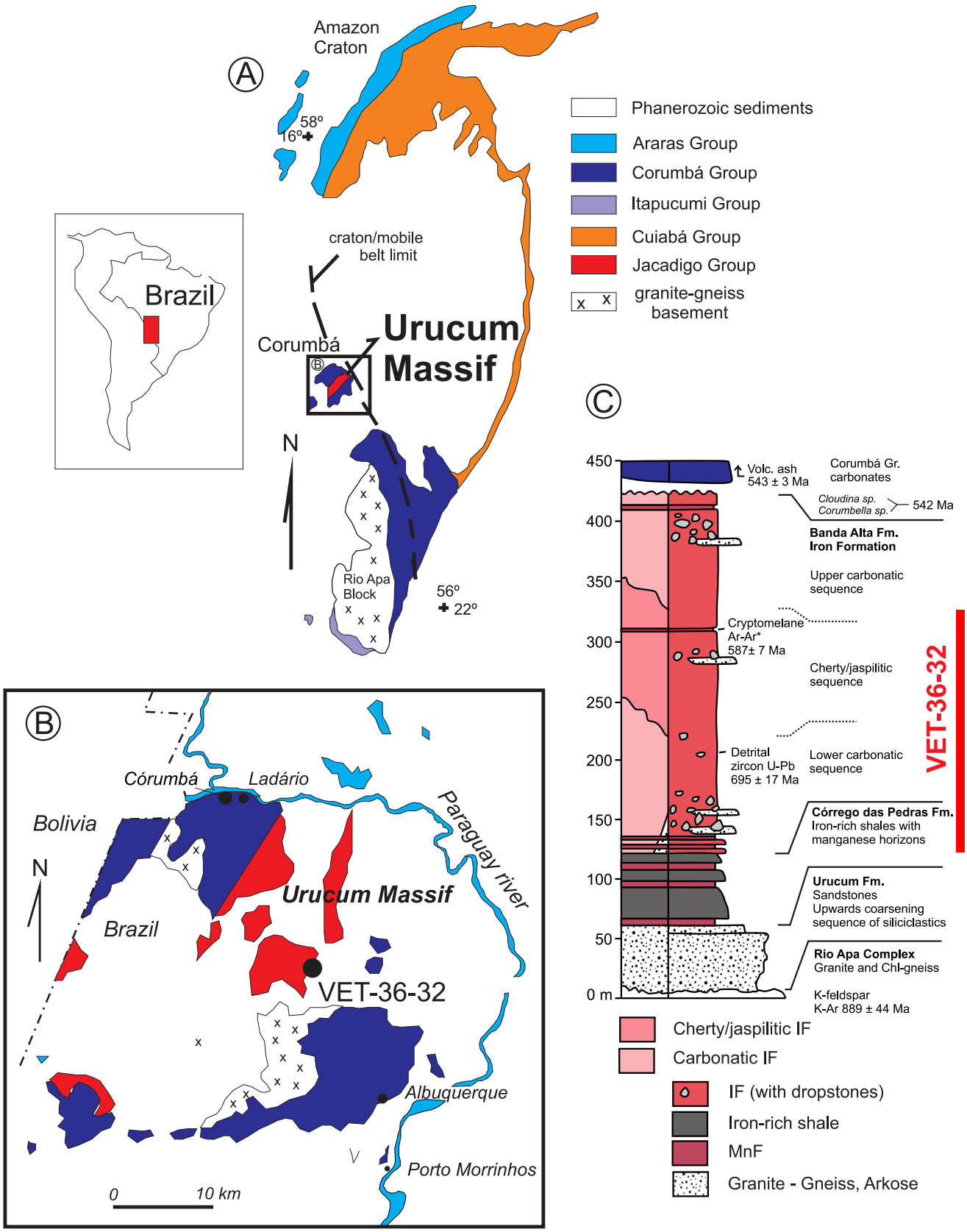

Fig. 1. (A) Simplified geological map showing portion of the Amazon Craton, marking the area of the Urucum Massif depicted in (B). (B) Local geology of the Corumbá area (modified and simplified from Arting et al., 2023). Location of drill hole VET-36-32, from which iron-rich mesoband samples have been analyzed herein, is indicated. (C) Stratigraphic profile, showing known radiometric ages (Babinski et al., 2013; Frei et al., 2017; Piacentini et al., 2013). The approximate section covered by the VET-36-32 drill core is marked with a red bar. Details see text. (For interpretation of the references to colour in this figure legend, the reader is referred to the web version of this article.)

signatures in sub-oxic and anoxic continental margin sediments, representing the primary output archives of Cd from the ocean (Heinrichs et al., 1980; Little et al., 2015; Rosenthal et al., 1995a; Rosenthal et al., 1995b; van Geen et al., 1995), to a large degree balance the Cd input sources and Cd in deep ocean waters. These sediments receive their light isotope signature by burial of organically-bound Cd (Janssen et al., 2019) and/or by burial of cadmium sulfide (CdS) in the presence of aqueous hydrogen sulfide (Bryan et al., 2021; Chen et al., 2021; Druce et al., 2022; Frei et al., 2020; Frei et al., 2021; Guinoiseau et al., 2019; Janssen et al., 2014; Plass et al., 2020). In addition, stripping of Cd by Fe—Mn oxides in pelagic clays, Fe—Mn crusts and nodules, iron oxyhdroxides and incorporation into marine carbonates (Boyle, 1988; Frederiksen et al., 2022a; Frederiksen et al., 2024; Frederiksen et al., 2022b; Horner et al., 2011; Rehkämper et al., 2012; Rosenthal et al., 1995a; Schmitt et al., 2009; van Geen et al., 1995; Wasylenki et al., 2014; Yan et al., 2021) are minor sinks in the Cd cycle. Cd isotope studies of BIFs formed during the Archean and Proterozoic are essentially lacking, despite the adsorptive property of Cd onto iron oxides and iron oxyhydroxides being known for quite some time (Benjamin and Leckie, 1981a, 1981b; Cowan et al., 1991; Liu et al., 2021; Petersen et al., 1993; Randall et al., 1999; and many others).

1.2. Geological setting

The geology of the Corumbá region (Fig. 1A,B) has been described in previous publications (Freitas et al., 2011; Piacentini et al., 2007; Piacentini et al., 2013; Trompette et al., 1998), and the tectonic, stratigraphic, structural and textural relations were summarized by Viehmann et al. (2016), Angerer et al. (2016), Freitas et al. (2011), and more recently, by Polgári et al. (2021) and Hiatt et al. (2020). Likewise, we refer to detailed descriptions of the mineralogy and sedimentology of the Urucum IF contained in the articles by the aforementioned authors.

The Neoproterozoic rocks in the Urucum district belong to the Jacadigo Group which forms part of the Río Apa Block of the southernmost part of the Amazonian Craton (Fig. 1A, B). The Jacadigo Group sediments were deposited in a rift to shelf setting (Trompette et al., 1998). They are unconformably overlain by late Ediacaran limestones and dolostones pertaining to the Corumbá Group (Almeida, 1965; Gaucher et al., 2003; Hiatt et al., 2020; Morais et al., 2021; Walde et al., 2015).

The stratigraphic relationships, lithological descriptions and geochronological details of the Jacadigo Group (Fig. 1C) have been described in chapter 3 of the recent publication by Árting et al. (2023). A summary of these details is contained in appendix A of the supplementary material.

2. Materials and methods

2.1. Samples

Samples were taken at 10-m intervals in iron-rich layers from drill core STCR-DD-36-32 (Vectorial Ltd.; W57°31′58.30″, S19°14′59.98″), a borehole at the Santa Cruz deposit, Morraria Grande (M. Grande;Fig. 1A, B). Great care was taken to avoid any arkose interbeds. Hematite bands (referred to as mesobands herein) were carefully separated from the drill core pieces using a diamond saw. The mesobands were then powdered in an agate mill. Two representative drill core pieces with hematite mesobands are depicted in Fig. 2. The mesoband samples are labeled "VETRIA" and are incrementally numbered with sampling depth. They correspond to the "VET" samples in the study of Árting et al. (2023) but represent newly separated mesobands from the same pieces of drill core. Major element compositions of continuous core samples referred to in this work are core logging data performed by Vectorial Ltd. mining company. The respective results have recently been reported in Table S1 of Árting et al. (2023).

2.2. Selected major and trace element analyses

Trace element concentrations were determined using solution ICP-MS (Inductively Coupled Plasma Mass Spectrometry). Aliquots of the powdered samples (50 mg) were dissolved in 3 mL 6 N HCl to match the dissolution of the mesoband samples for Cr and Cd isotope analyses. This

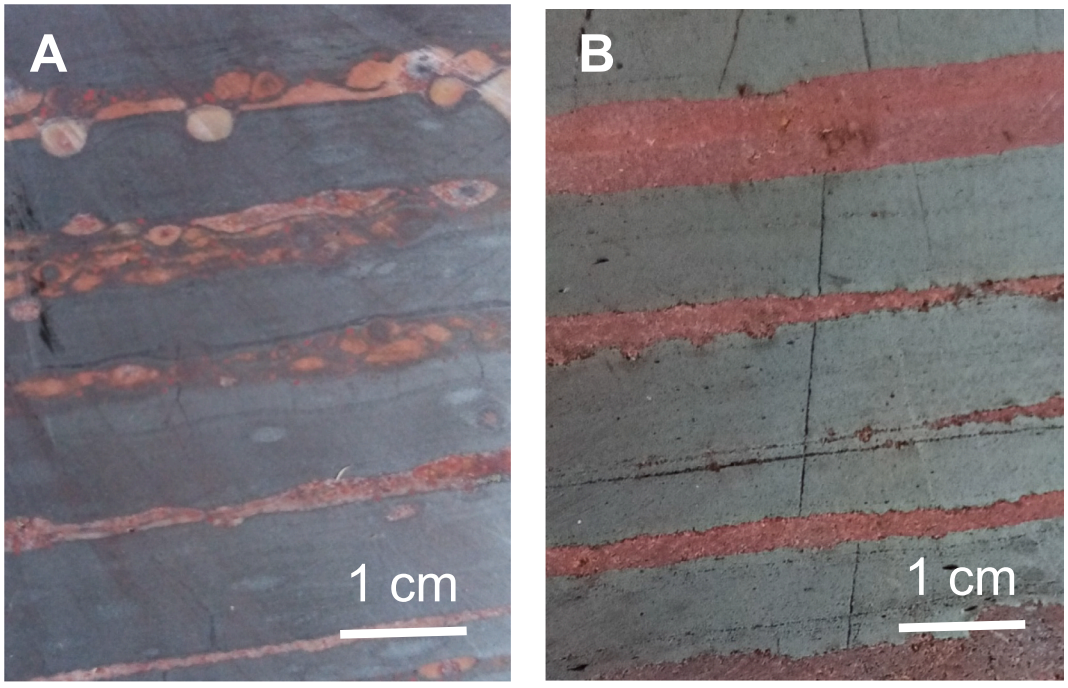

Fig. 2. Representative drill core sections (cut slabs) from which respective hematite mesobands were separated for analyses. A. Sample VETRIA-20; nodular IF with carbonaceous ooids from the lower part of the Banda Alta Formation (212.00 m). B. Sample VET-05: Banded cherty/jaspilitic IF from the upper part of the Banda Alta Formation with leached carbonates (38.30 m).

dissolution prevented the formation of iron oxyhydroxide precipitates and enabled a complete dissolution of the hematite and carbonates, without strongly attacking relict siliciclastic components. After centrifugation, the supernatants were evaporated to incipient dryness and re-dissolved in 0.5 M HNO_3 + 0.01 M HF. The ICP-MS quadrupole instrument iCAP-Q from Thermo Scientific was used for the determination of the elements. KED (Kinetic Energy Discrimination) instrumental mode was selected for the analysis using ultrapure He as collision gas for the suppression of potentially interfering molecular ions. Prior to analysis, all leachates, standards and reference solutions were diluted twofold with the internal standard. An internal standard solution of 10 μg/L In in 0.32 M HNO_3 was prepared of de-ionized water and nitric acid of sub boiling quality. Four separate sets of calibration standards were prepared gravimetrically from stock solutions of mixed standards (Inorganic Ventures) covering REE, refractory elements in HNO_3/HF, additional elements, and major elements. Two different instrumental methods were set up to cover the elements. NIST 1643f and a diluted Reagecon ICP-Multielement Standard with 23 elements was used as calibration verification standard. Two iron formation standards (GIT-IWG; Govindaraju, 1984; FER-1; Abbey et al., 1983) and dolomite JDo-1 (Imai et al., 1996) were analyzed as internal control samples.

2.3. Ion chromatographic separation of chromium and cadmium

In order to obtain Cr and Cd isotope data from one and the same dissolved sample, we developed an ion chromatographic separation technique which allows for a combined, successive and high purity separation of these two elements. One of the challenges was the very low Cd concentrations ([Cd]; range between 1 and 7 ng/g) opposing three orders of magnitude higher Cr concentrations ([Cr]); range between 1 and 15 μg/g). In order to allow for a combined Cr—Cd double spiking, adequate liquid aliquoting of the sample solutions was therefore necessary. Powdered samples (4 × 2 g) were spiked with adequate amounts of a $^{106\text{-}108}$Cd double spike, whereby one 2 g aliquot was additionally spiked with an appropriate amount of $^{50\text{-}54}$Cr double spike. The 2 g sub-samples were attacked with 45 mL of 6 M HCl in 50 mL Savillex™ Teflon beakers placed on a hotplate at 140 °C for 48 h. After cooling the digestions to room temperature, the samples were transferred to 50 mL centrifuge tubes and centrifuged for 5 min at 4000 rpm. The supernatant was back transferred to 250 mL Savillex™ beakers and dried down on a hotplate. Then, the samples were dissolved in 200 mL of 0.7 M HCl.

2.3.1. Cd separation

The 200 mL of 0.7 M HCl sample solutions were passed over 10 mL Bio-Rad™ Poly-Prep® (PP) extraction columns charged with 2 mL of 200–400 mesh Bio-Rad™ AG-1 × 8 anion resin. Only the eluates of the combined Cr—Cd double spiked aliquots were collected, as they contain the Cr portion of the samples. After loading and fully passing the sample solution through the column, using expansion funnels to accommodate the 200 mL sample solutions, the following acid rinses were added to the columns: 22 mL of 0.7 M HCl, 6 mL of 1 M HCl, 6 mL of 2 M HCl, 6 mL of 8 M HCl, 11 mL 0.2 M HBr/0.5 M HNO_3, and 2 mL of 2 M HNO_3. Finally, Cd was extracted from the resin with 13 mL of 2 M HNO_3 into 17 mL Savillex™ beakers and the Cd eluate was dried down on a hotplate. This first column step was modified after recipes in Ripperger and Rehkamper (2007) and Gault-Ringold (2011).

A clean-up of the first Cd fraction was achieved over disposable 1 mL pipette tip columns fitted with a frit and charged with 300 μL of 100–200 mesh Bio-Rad™ AG1x8 anion resin. For this purpose, the dried Cd-containing sample from the first column was dissolved in 0.5 mL of a 0.2 M HBr-0.5 M HNO_3 mix, and the remaining matrix elements were washed out with 1.5 mL of the same mix, followed by 1.5 mL of a 0.03 M HBr-0.5 N HNO_3 mix, then by 0.7 mL of 1 M HCl and by 0.2 mL of de-ionized water. Cd was then collected with 3.5 mL of 0.25 M HNO_3 and dried down. This column clean-up procedure followed that first reported by Frei et al. (2020). A pass over this clean-up column step was repeated once more, using the same resin charged pipette tip columns. The final Cd separates were very pure, essentially matrix-free, and well-suited for TIMS mass spectrometric analysis. Total procedural Cd yields were in the order of ca. 70% and near completely constrained to the first column separation in which the massive Fe matrix is being removed.

2.3.2. Cr separation

The dried down double spiked Cr sample aliquots collected as eluates from the first Cd separation step were re-dissolved in 20 mL of 6 M HCl and passed over 20 mL stem volume Bio-Rad™ Econo-Pac® columns charged with 15 mL of 100–200 mesh Bio-Rad™ AG1x8 resin following (Frei et al., 2009). This step efficiently removes the Fe matrix. The Fe-free, Cr containing eluates were collected in 23 mL Savillex™ Teflon beakers and dried down.

Then, samples were re-dissolved in 20 mL of de-ionized water to which a few drops of concentrated HCl and 0.5 mL of a 1 N ammonium peroxydisulfate solution were added. These solutions were then boiled with closed lids in a block on a hotplate at 130 °C for 1 h to ensure oxidation of Cr(III) to Cr(VI). Upon cooling to room temperature, the sample solution was then passed over Bio-Rad™ PP extraction columns charged with 2 mL anion resin (Bio-Rad™ AG1x8, 100–200 mesh). Cr (VI), retained in the resin, was released by reduction to Cr(III) with the help of 10 mL of 0.1 M HNO_3 doped with 3 drops of concentrated H_2O_2 into 12 mL Savillex™ Teflon beakers. After drying of this eluate on a hotplate, the sample was re-dissolved in 200 μL of 6 M HCl, then diluted with 2 mL de-ionized water and passed over 2 mL of cation exchange resin (AG 50 W-8, 200–400 mesh) charged Specra/Chrom® disposable columns equipped with a 15 μm filter size frit. The cation column extraction procedure followed a the slightly modified recipe of Bonnand et al. (2011) and Trinquier et al. (2008). With applying a three-step ion chromatographic column procedure, we obtain highly pure Cr separates. Disturbing cations and anions are efficiently removed from the sample solutions during the oxidation-reduction step in the anion chromatographic separation. Total procedural Cr yields were in the order between 60 and 70% and mainly dominated by Cr losses during the final cation exchange column separation.

2.4. Mass spectrometric analyses of Cd and Cr isotopes

Cr separates were loaded on Re-filaments with 1.5 μL of silicic acid (Gerstenberger and Haase, 1997) and 0.5 μL of 1 N H_3PO_4 and 0.5 μL of saturated H_3BO_3. Further details are contained in Døssing et al. (2011), Frei et al. (2016) and Paulukat et al. (2015).

Cd separates were also loaded onto outgassed Re-filaments in a 2.5 μL mix of 0.5 N H_3PO_4, silicic acid (Gerstenberger and Haase, 1997) and 0.5 N H_3BO_3 in volume ratios of 1:8:1.

All samples were subsequently measured on a IsotopX PHOENIX TIMS operating in static multi-collection mode at the Dept. of Geosciences and Natural Resource Management, University of Copenhagen. Running temperatures were between 1020 and 1180 °C. Data reduction for the natural and instrumental mass-dependent isotope fractionation used own external double-spike algorithms, assuming an exponential fractionation law, combined with the Newton-Rhapson method implemented in an in-house Python 3 program (Rudge et al., 2009, and references therein).

The statistical uncertainties are based on reducing each measurement cycle (6 s integration time), over a total of 120 cycles per analysis, with baseline measurements of 6 s integration time at ±0.5 amu after every block of 20 cycles. The analytical blanks for Cr and Cd were in the order of 1.2–1.5 ng for Cr, and 20–40 pg for Cd, amounts which, if compared to Cr and Cd sample loads of > ~2 μg and > ~20 ng, respectively, insignificantly affected the final Cr and Cd isotope signatures of the samples. The ^{106}Cd—^{108}Cd double spike was calibrated against "zero-delta" NIST 3108 set to yield $\delta^{114}Cd = 0$, and the ^{50}Cr—^{54}Cr double spike was calibrated against NIST 979 to yield δ^{53}Cr

= 0.

Variations of Cd isotope compositions are expressed as average δ^{114}Cd values (‰) ± double standard deviation (2σ) from repeated runs (abbreviation for $\delta^{114/110}$Cd, i.e., the deviation of ^{114}Cd/^{110}Cd in parts per 1000) from reference material NIST 3108:

$$\delta^{114}\mathrm{Cd}\ (‰) = \left[\left(^{114}\mathrm{Cd}/^{110}\mathrm{Cd}_{\mathrm{sample}}/^{114}\mathrm{Cd}/^{110}\mathrm{Cd}_{\mathrm{NIST3108}}\right) - 1\right] \times 10^3 \quad (1)$$

The Cr isotope compositions of the samples were determined as the average of repeated analyses and are reported in per mil (‰) ± double standard deviation (2σ) relative to the international reference and zero delta standard NIST 979, reported as.

$$\delta^{53}\mathrm{Cr}\ (‰) = \left[\left(^{53}\mathrm{Cr}/^{52}\mathrm{Cr}_{\mathrm{sample}}\right)/\left(^{53}\mathrm{Cr}/^{52}\mathrm{Cr}_{\mathrm{NIST979}}\right) - 1\right\} \times 10^3 \quad (2)$$

In cases where the 2σ errors were below the long term external 2σ reproducibility of 0.09‰ (n = 105, 2σ), for double spiked NIST 979, measured under the same conditions as the samples with ^{52}Cr beams between 500 mV and 1 V, we employed and assigned that external reproducibility error to the respective analyses.

Repeated double spiked NIST 3108 analyses at 300 mV, 600 mV and 1 V beam intensities of ^{112}Cd yielded reproducibilities of ±0.062, ±0.034, and ±0.019 δ^{114}Cd units (2σ; n = 15), respectively. Repetitive interspersed analyses of MCd ("Münster cadmium") and BAMIO12 reference solutions yielded δ^{114}Cd values of 4.66 ± 0.085 (2σ; n = 10) and − 1.36 ± 0.06 (2σ; n = 9), respectively, in accordance with values measured by other laboratories (Abouchami et al., 2013). Reproducibility of sample isotopic compositions was performed by multiple dissolutions and mass spectrometric analyses of the JDo-1 dolomite standard (Imai et al., 1996) and the GIT-IWG iron formation standard, both of which are not certified for δ^{53}Cr and δ^{114}Cd values. Four separate dissolutions of these materials yielded δ^{53}Cr = 1.72 ± 0.08 ‰ and δ^{114}Cd = 0.03 ± 0.06 ‰ (2σ), and δ^{53}Cr = 0.03 ± 0.03 ‰ (2σ) and δ^{114}Cd = 0.21 ± 0.04 ‰ (2σ), respectively, in agreement with values recently published by Frederiksen et al. (2022b) for JDo-1, and with δ^{53}Cr values published by Frei et al. (2016) for GIT-IWG.

3. Results

3.1. Selected major elements

Selected major and trace element data measured on 6 N HCl attacks of the hematite mesobands are reported in Table A1. Stratigraphic distribution of SiO_2, CaO + MgO and Al_2O_3 concentrations in the continuous bulk core samples (reported in Table S2 of Árting et al. (2023)) are plotted in Fig. 3 for comparative purpose.

Between ca. 300–350 m depth, in the basal section of the Banda Alta

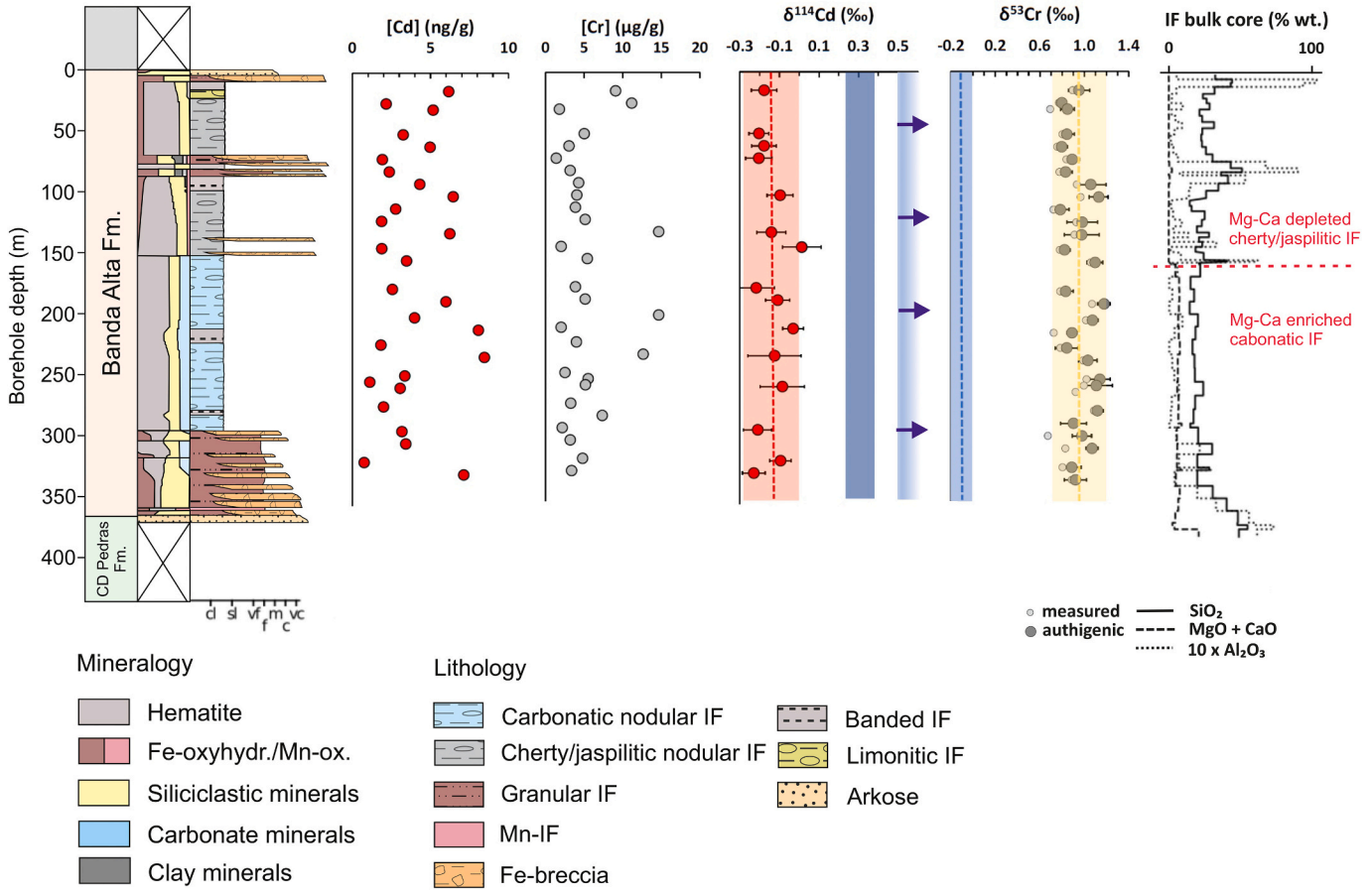

Fig. 3. Lithological log of Vectorial drillcore VET-36-32 indicates layers with detrital (siliciclastic) input, mobilization of IF (Fe-breccia) and (limonite) alteration. Geochemical variations in iron-rich mesobands: [Cd] and [Cr], δ^{114}Cd and δ^{53}Cr (measured: small light grey circles; authigenic: large dark grey circles), and bulk core compositions (in % wt.) of SiO_2, MgO + CaO, and Al_2O_3 (enhanced by factor 10), provided by Vectorial Mine Ltd. Dark blue band in the δ^{114}Cd log marks the range of deep modern ocean seawaters of 0.35 ± 0.12 ‰ (Conway and John, 2015a; Conway and John, 2015b; Janssen et al., 2017; John et al., 2018; Ripperger et al., 2007; Sieber et al., 2019; Xie et al., 2017); Gradient blue filled band with blue arrows marks the composition of δ^{114}Cd in modern surface waters (~0.5–1 ‰; (Abouchami et al., 2011; Abouchami et al., 2014; Xue et al., 2013; Yang et al., 2014, and others). Blue band and blue dashed line in the δ^{53}Cr log mark the range and average, respectively, of solid Earth reservoir δ^{53}Cr of 0.12 ± 0.10 ‰ as defined by Schoenberg et al. (2008). cl = clay, slt = silt, vf = very fine, f = fine, m = medium, c = coarse, vc = very coarse. For details and interpretation refer to text. (For interpretation of the references to colour in this figure legend, the reader is referred to the web version of this article.)

Formation, there is a gradual transition from the siliciclastics of the underlying Corrego das Pedras Formation, to carbonatic IF. This is shown by the gradual decrease up to 320 m in concentrations of SiO_2 and Al_2O_3 in the mining companies' continuous bulk core geochemical data (Fig. 3). In this interval there is a lack of pure hematite mesobands. This basal interval is succeeded by two major IF intervals (Fig. 3). The first interval (at ~300–150 m depth) is dominated by carbonatic IF with bulk CaO + MgO ~ 10% wt., Al_2O_3 < 1% wt., and bulk SiO_2 < 20% wt. The appearance of carbonates shows as a jump, particularly in the bulk core data profile, towards higher CaO + MgO and lower Fe and SiO_2 concentrations below ~160 m depth. (Fig. 3). This compositional transition is also depicted in corresponding changes in the hematite mesoband compositions reported herein (Fig. 4). The second pronounced interval above ~150 m depth is characterized by cherty/jaspilitic IF, with low CaO + MgO < 1% wt. This topmost interval is also marked by the reappearance of interspersed gravity flow deposits. These gravity flow deposits show in the continuous bulk core profile as horizons with increased bulk core Al_2O_3 (up to 10% wt.) contents and concomitantly fluctuating SiO_2 concentrations varying between 30 and 50% wt. (Fig. 3).

The hematite mesobands analyzed herein (Table A1; supplementary material) have [Fe] concentrations ranging between 33 and 66% wt., and [Ca + Mg] concentrations ranging between 0.03 and 6.54 wt%, with significantly higher [Ca + Mg] concentrations in the basal (~300–150 m) part of the profile, analogue to the bulk core distinctions (cf. Figs. 3,4). The elevated Al_2O_3 observed in bulk samples of the upper part of the Banda Alta Fm. (Fig. 3; Table S1 in Árting et al., 2023) are not reflected in the hematite mesoband samples studied herein from within the upper portion of the Banda Alta Formation (cf. Table A1). Instead, [Al] concentrations unsystematically scatter between 92 and 1872 μg/g in the hematite mesobands throughout the drill core (Table A1), attesting to only small contamination of the analyzed hematite mesobands by detrital silicate components.

3.2. Rare earth element and yttrium patterns

Rare Earth Element (REE) and yttrium (Y) concentrations are part of Table A1 which lists the complete trace element concentrations of hematite mesoband samples studied herein. Shale normalized REY anomalies are reported using the recommended formulae of Bolhar et al. (2004) and Bau and Dulski (1996). These formulae use the geometric mean to estimate the unfractionated reference concentration and normalized (suffix N in equations below) to Post-Archean Australian Shale (PAAS;(McLennan, 1989;Taylor and McLennan, 1985):

$$Eu/Eu^{*} = Eu_N \cdot Sm_N^{-2/3} \cdot Tb_N^{-1/3} \quad (3)$$

$$Ce/Ce^{*} = Ce_N \cdot Pr_N^{-2} \cdot Nd_N \quad (4)$$

$$Pr/Pr^{*} = Pr_N^{-1} \cdot (0.5 \cdot Ce_N + 0.5 \cdot Nd_N) \quad (5)$$

The abundance of Y relative to PAAS-normalized REE patterns is evaluated by the deviation of the Y—Ho ratio from the chondritic value (ca. 28; McDonough and Sun, 1995). Positive deviations indicate the faster scavenging of Ho relative to Y in seawater by distinctly different complexation with inorganic ligands (mainly carbonate ions) and

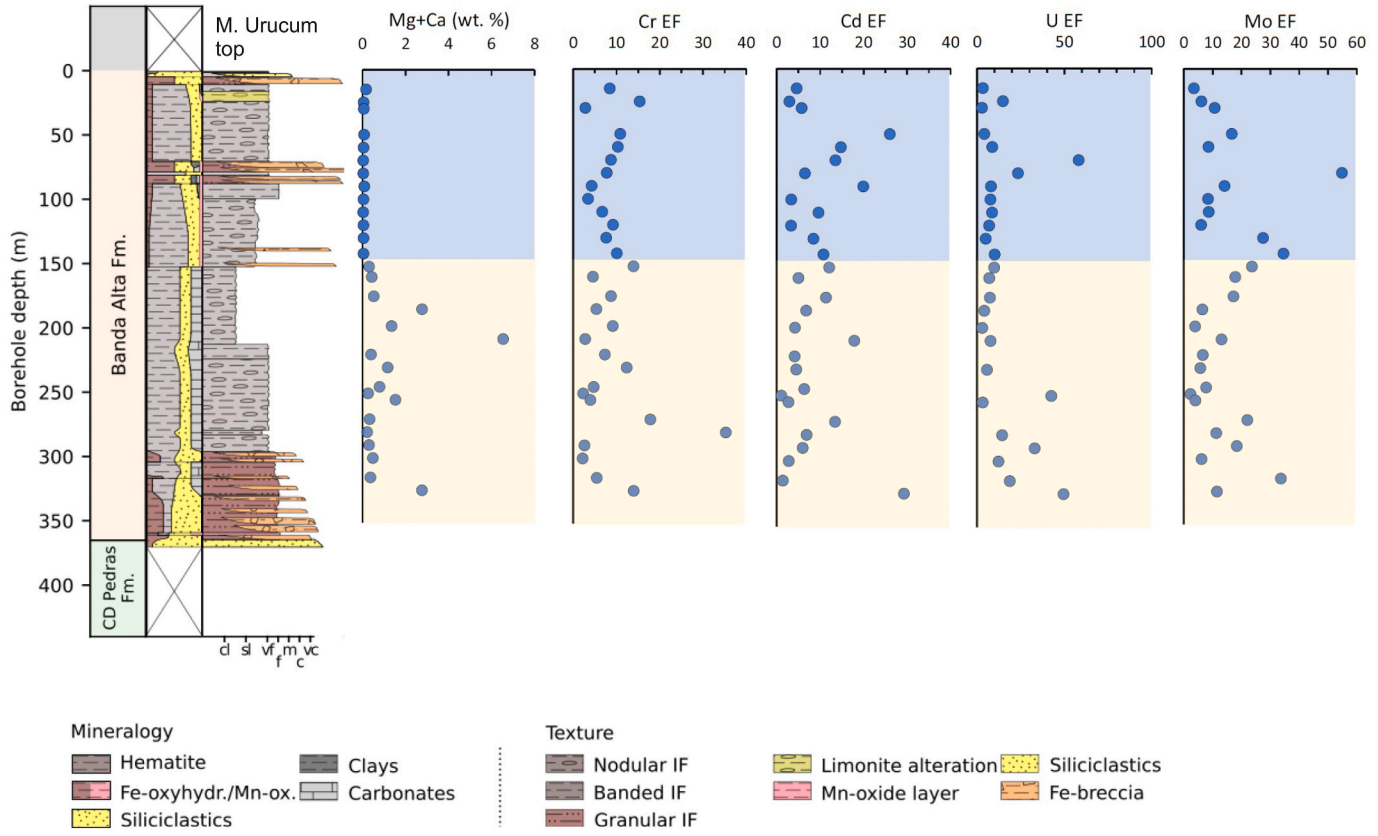

Fig. 4. Lithological log of Vectorial drillcore VET-36-32 as in Fig. 3. Geochemical variations in iron-rich mesobands: Mg + Ca (wt.%) distinguishes the lower, carbonatic part (underlined in bright yellow panels) from the upper cherty/jaspilitic part (underlined in bright blue panels) of the Banda Alta Formation. Enrichment factors (EF) of Cr, Cd, U and Mo as defined in the text. Relatively strong variation of Cr EF and Cd EF, in combination with only small variation in $\delta^{53}Cr$ and $\delta^{114}Cr$ (Fig. 4) respectively, are interpreted to support quantitative removal of dissolved Cr and Cd from the Jacadigo Basin surface waters into iron formation. For details refer to text. cl = clay, slt = silt, vf = very fine, f = fine, m = medium, c = coarse, vc = very coarse. (For interpretation of the references to colour in this figure legend, the reader is referred to the web version of this article.)

subsequent different adsorption of soft organic ligands onto the surface of particulate matter (Nozaki et al., 1997). Differential adsorption of Y and Ho during weathering related mobilization and fluvial transport to the ocean has shown to be minimal and therefore freshwater transport has a minimal impact on the differentiated behavior of these two elements in seawater (Bau, 1999). Shale normalized REY patterns are light rare earth element (LREE) depleted (Pr/Yb_{PAAS} 0.19–1.09 (average 0.40 ± 0.42; 2σ, n = 30; Table A1), exhibit negative Ce/Ce* (0.52–1.00; average 0.79 ± 0.22; 2σ, n = 30; Table A1) and are characterized by circumneutral Eu/Eu* (0.99–1.15; average 1.06 ± 0.07; 2σ, n = 30; Table A1). REY patterns, grouped into samples from the lower (carbonatic) and upper (cherty/jaspilitic) sequence, are plotted in Fig. 5A. Shape-wise, and with respect to the magnitude of negative Ce-anomalies, the patterns from the lower and upper Banda Alta Formation cannot be distinguished from each other. The REY patterns in Fig. 5A differ merely by their overall total REY concentrations. Using the Pr/Pr* vs. Ce/Ce* discrimination diagram of Bau and Dulski (1996) to delineate true negative Ce-anomalies against those compromised by potential La enrichments (Fig. 5B), we note that 9 of the 30 mesoband samples lie outside of field IIIb characterizing true negative Ce anomalies (Bau and Dulski, 1996). Y/Ho ratios vary between 28 and 50 (average 37 ± 10; 2σ, n = 30; Table A1), with most samples exhibiting a positive ratio (≥ 28). Two samples (VETRIA 024, 029) are characterized by chondritic values (Table A1). There is a trend towards increasing Y/Ho stratigraphically upward (Fig. 5C), consistent with a decreasing admixture of freshwater and with a general transgressive sequence in the Banda Alta Formation (e.g., Angerer et al. (2016)).

3.3. Redox sensitive trace elements

Upon oxidative release from continental landmasses during weathering processes, the redox sensitive elements Cr, Mo and U enter the oceans in their oxidized states Cr(VI), Mo(VI) and U(VI) (Algeo and Maynard, 2008; Frei et al., 2014; Partin et al., 2013). Reduction of Cr (VI) to Cr(III) by upwelling Fe^{2+} fertilized bottom waters is expected to be efficient and complete. Cr(III) is thereby incorporated into colloidal, iron oxide precursor phases (among others, iron oxyhydroxides; Frei et al., 2009). Similarly, dissolved soluble Mo(VI) present as molybdate (MoO_4^{2-}) is slowly removed from the surface waters by incorporation into Mn-oxide particle. Under euxinic conditions, however, Mo is present as the thiomolybdate ion. Under these conditions then, Mo is particle reactive and sequestered by Fe—Mn oxides, Fe-sulfides, organic material and clay minerals (Algeo and Tribovillard, 2009). Similar to Mo (VI), soluble U(VI) is adsorbed by ferric oxyhydroxides as an oxidized

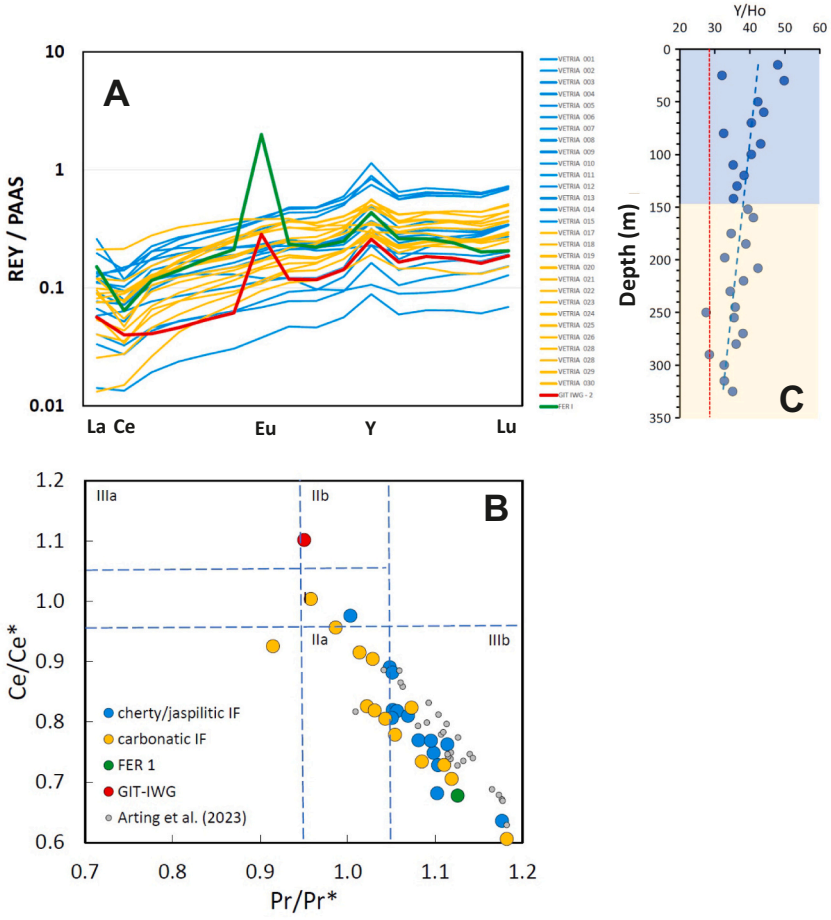

Fig. 5. (A) Shale normalized Rare Earth Yttrium (REY) patterns and Y/Ho log of iron-rich mesobands from the Banda Alta Formation. Yellow patterns are samples from the lower, carbonatic part, blue patterns are from the upper, cherty/jaspilitic part. Reference samples GIT IWG (Eoarchean BIF from the Isua Greenstone Belt, W Greenland) and FER 1 (Proterozoic BIF from Austin Brook near Bathurst, New Brunswick, Canada) are indicated in red and green patterns, respectivley. REY patterns of mesobands from M. Grande studied herein are subparallel and seawater-like, exhibiting predominantly negative Ce anomalies but lack Eu anomalies. (B) Y/Ho ratios depict a trend towards higher values stratigraphically upward, a feature which we interpret to reflect increasing open seawater contribution to the semi-restricted Jacadigo Basin during a transgressive cycle, potentially related to glacier melt down. (C) Discrimination diagram which distinguishes "true" from "false" negative Ce anomalies (labeled fields correspond to those in Bau and Dulski, 1996). Twenty one of 30 mesoband samples plot within field IIIb characterizing true negative Ce anomalies indicative of oxidized surface waters. Data of iron-rich mesobands published by Árting et al. (2023) are plotted for reference. For details refer to text. (For interpretation of the references to colour in this figure legend, the reader is referred to the web version of this article.)

species, and through subsequent reduction to U(IV) it is incorporated in minerals, such as for example goethite (Hsi and Langmuir, 1985; Liger et al., 1999; Partin et al., 2013).

In order to estimate the relative enrichment of the redox sensitive trace elements in the IF mesobands analyzed herein relative to continental sources, we calculated Enrichment Factors (EF) as follows:

$$Me_{EF} = \frac{\left[C_{redox}/C_{ref}\right]_{sample}}{\left[C_{redox}/C_{ref}\right]_{source}} \quad (6)$$

Me_{EF} is the metal EF, and C_{redox} and C_{ref} stand for the concentrations of the trace element of interest and a reference element, respectively. We use Al as an insoluble and abundant major reference element as we believe that it adequately reflects detrital silicate phases in our chemical sediments. We assume a PAAS-like composition to represent such a co-sedimented siliciclastic fraction, with 100,026 mg/kg Al, 110 mg/kg Cr, 1.5 mg/kg Mo, and 3.1 mg/kg U (Taylor and McLennan, 1985). In addition, we report Cd EF (Table A1) using a LOES-like Cd concentration of 0.124 mg/kg as reference (Schmitt et al., 2009).

The Cr, Mo, U and Cd EFs are plotted in Fig. 4 along with the Morro Grande stratigraphic column. The EFs are strongly positive, but highly variable. They appear not to reflect the distinction between carbonatic IF (elevated [Mg + Ca]) predominant in the lower part, and cherty/jaspilitic IF (low [Mg + Ca]) in the upper part of the Banda Alta Fm.; Fig. 3). EFs also do not show correlation with [Fe] of the mesobands (not plotted here). Overall, the hematite mesoband samples studied herein are similarly enriched in U, Cr and Mo (Fig. 6A, B), but with some samples exhibiting significant U EF over Mo EF (Table 1, Fig. 6A). When compared to EFs of these elements in IF mesobands reported in previous studies (e.g. (Árting et al., 2023)), we notice a shift of the data reported in the latter study towards increased Cr EF relative to Mo EF (Fig. 6B). This is explained by the fact that Árting et al. (2023) used a smaller [Cr] (54 mg/kg) as reference detrital normalization value than the PAAS value of 110 mg/kg used herein. Our data presented herein are compatible with computed Mo EF and U EF from the data reported by Viehmann et al. (2016) on IF and MnF from various drill cores from the Urucum ore district and those of iron-rich mesobands from Morro Grande analyzed by Árting et al. (2023) (plotted in Fig. 6A for comparison). While some of our data points clearly show enrichments of Mo relative to U (Mo EF plot above the 1:1 reference line in Fig. 6A), a feature which is not as pronouncedly observed in the Árting et al. (2023) data, a number of samples also exhibit a tendency to show elevated U EF relative to Mo EF as also seen in the mesoband data set of Árting et al. (2023).

3.4. Cr-isotopes

Chromium isotope signatures of the hematite mesobands are in the range from $\delta^{53}Cr = +0.67$ ‰ - +1.09 ‰ (Table 1), ca. 0.1‰ higher than hematite mesobands from the same drill core sections analyzed by Árting et al. (2023). This small discrepancy is ascribed to the use of different acid attacks (*aqua regia* vs. 6 M HCl) of the sample powders and to the different detrital siliciclastic contamination in the hematite mesobands studied by Árting et al. (2023) versus samples studied herein. The 6 M HCl attack employed here is apparently beneficial for improving the authigenic over siliciclastic signal as siliciclastic components are less affected than by the more aggressive *aqua regia* attacks used in the latter study. This is corroborated by the lower [Al] measured in the sample solution compared to [Al] in solutions produced by Árting et al. (2023) (cf. Table A1 vs. Table S1 in the latter study). Long-term stratigraphic variations in the measured $\delta^{53}Cr$ signals are small (Fig. 4). There is a lack of significant correlation between $\delta^{53}Cr$ values and [Cr] and major element concentrations, such as [Al] and [Ti], which discriminate against siliciclastic detrital contamination (not plotted here). Calculation of authigenic Cr isotope compositions ($\delta^{53}Cr_{auth}$) was done according to the algorithm used by Gilleaudeau et al. (2018)

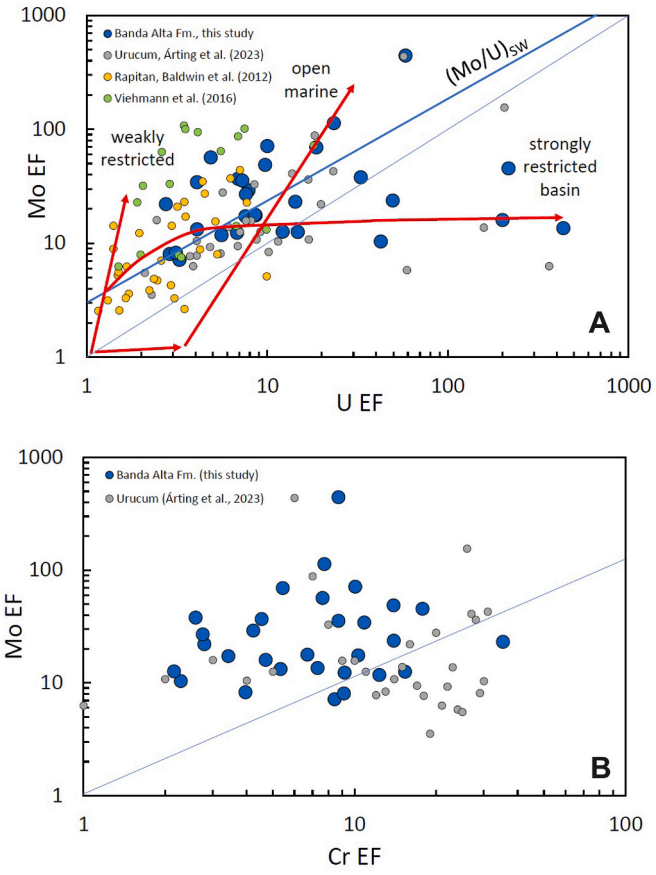

Fig. 6. Enrichment factors for redox sensitive elements. (A) U_{EF} against Mo_{EF} (diagram adapted from Algeo and Tribovillard, 2009) with red arrows pointing to three types of modern redox-sensitive basins. Data plotted are iron-rich mesobands from this study (dark blue big circles), iron-rich mesobands from Árting et al. (2023) (small grey filled circles), pure IF samples from Viehmann et al. (2016) and, for reference, Rapitan IF samples from Baldwin et al. (2012). Blue thick solid line marks the modern seawater Mo/U_{SW} trendline. The thin blue line is the 1:1 trend line indicated for reference purpose. The array of data from Urucum indicates transitions from weakly restricted to strongly restricted basin evolutionary trends, with dominant open marine influence. For details refer to text. (B) Cr_{EF} against Mo_{EF} in iron-rich mesobands from this study (large blue filled circles) and from Árting et al. (2023). The data from the work presented herein irregularly scatter around the 1:1 line, which indicates a similar oxidative removal from the continental landmass and reductive stripping into iron oxyhydroxides. Shift of iron-rich mesoband data published by Árting et al. (2023) towards elevated CR EF values is due to use of a lower [Cr] for detrital siliciclastics in the Al-normalization of their data relative to PAAS values used herein. Mo EF are all recalculated using a Mo concentration of PAAS of 1.5 mg/kg (Taylor and McLennan, 1985). For details refer to text. (For interpretation of the references to colour in this figure legend, the reader is referred to the web version of this article.)

specified below, assuming a fixed ratio between Cr and Al as an immobile reference element in the detrital component, and a more or less congruent partial dissolution of the two elements.

$$Cr_{det\ sam} = Cr_{PAAS}{}^{*}\ Al_2O_{3\ sam\ meas}/Al_2O_{3\ PAAS} \quad (7)$$

$$\%Cr_{det} = (Cr_{det\ sam}/Cr_{sam\ meas})^{*}100 \quad (8)$$

$$\delta^{53}Cr_{auth} = \left(\delta^{53}Cr_{meas} - \left(\delta^{53}Cr_{PAAS}{}^{*}\ (\%Cr_{det\ sam}/100)\right)\right)/(1-(\%Cr_{det\ sam}/100)) \quad (9)$$

The subscripts "sam", "meas", "det" and "auth", refer to sample, measured, detrital and authigenic, respectively.

Authigenic Cr isotope compositions($\delta^{53}Cr_{auth}$), detrital Cr

Table 1
Cr and Cd isotope signatures and Cr and Cd concentrations in hematite mesobands from the Banda Alta Formation.

Sample	Depth	δ^{53}Cr	2σ	[Cr] ICP	[Cr] ID	δ^{114}Cd	2σ	[Cd] ICP	[Cd] ID	[Al]	[Cr] det	%[Cr] det ID	%[Cr] auth ID	δ^{53}Cr auth ID	[Cd] det	%[Cd] det ID	%[Cd] auth ID	δ^{114}Cd auth ID
	m	‰		mg/kg	mg/kg	‰		ng/g	ng/g	mg/kg	mg/kg			‰	ng/g			‰
VETRIA-01	15	0.78	0.08	9.07	10.54	−0.38	0.06	5.57	6.16	978	0.48	4.6	95.4	0.83	0.055	1.0	99.0	−0.18
VETRIA-02	25	0.77	0.03	10.14	11.15			2.16	2.16	601	0.29	2.6	97.4	0.80	0.012	0.5	99.5	
VETRIA-03	30	0.69	0.06	1.89	1.78			4.37	5.16	616	0.30	17.0	83.0	0.86	0.029	0.7	99.3	
VETRIA-04	50	0.80	0.07	6.23	5.00	−0.40	0.05	2.84	3.24	522	0.26	5.1	94.9	0.85	0.015	0.1	99.9	−0.20
VETRIA-05	60	0.76	0.05	2.93	3.02	−0.38	0.06	4.73	4.97	259	0.13	4.2	95.8	0.80	0.012	0.2	99.8	−0.18
VETRIA-06	70	0.84	0.07	0.88	1.37	−0.40	0.07	1.54	1.91	92	0.05	3.3	96.7	0.87	0.002	0.1	99.9	−0.20
VETRIA-07	80	0.78	0.06	2.08	3.17			1.96	2.36	244	0.12	3.8	96.2	0.81	0.005	0.3	99.7	
VETRIA-08	90	0.93	0.14	4.22	4.27			3.22	4.31	909	0.45	10.4	89.6	1.06	0.036	0.2	99.8	
VETRIA-09	100	0.97	0.09	2.05	4.05	−0.30	0.07	2.26	6.45	545	0.27	6.6	93.4	1.04	0.032	1.4	98.6	−0.10
VETRIA-10	110	0.72	0.08	3.45	3.85			5.58	2.77	468	0.23	6.0	94.0	0.78	0.012	0.2	99.8	
VETRIA-11	120	0.93	0.14	5.90	5.12			2.39	1.86	584	0.29	5.6	94.4	0.99	0.010	0.4	99.6	
VETRIA-12	130	0.91	0.16	6.67	14.65	−0.34	0.07	8.34	0.00	796	0.39	2.7	97.3	0.94	0.045	0.5	99.5	−0.14
VETRIA-13	142	0.78	0.05	3.17	2.01	−0.19	0.10	3.82	1.87	287	0.14	7.0	93.0	0.85	0.005	0.1	99.9	0.01
VETRIA-14	152	1.06	0.07	4.77	5.40			4.65	3.46	311	0.15	2.8	97.2	1.09	0.010	0.2	99.8	
VETRIA-15	160	0.72	0.07	2.14	2.49					429	0.21	8.5	91.5	0.80				
VETRIA-16																		
V ETRIA-17	175	0.78	0.07	2.24	3.85	−0.42	0.09	3.28	2.56	234	0.11	3.0	97.0	0.81	0.005	0.2	99.8	−0.22
V ETRIA-18	185	1.07	0.06	4.28	5.12	−0.31	0.06	6.14	5.99	730	0.36	7.0	93.0	1.16	0.040	0.6	99.4	−0.11
V ETRIA-19	198	1.01	0.05	8.16	14.65			4.22	0.00	813	0.40	2.7	97.3	1.05	0.029	0.7	99.3	
V ETRIA-20	208	0.72	0.04	1.78	2.01	−0.23	0.05	7.13	8.06	588	0.29	14.4	85.6	0.87	0.043	0.3	99.7	−0.03
V ETRIA-21	220	0.78	0.10	3.39	3.99			2.15	0.00	422	0.21	5.2	94.8	0.83	0.007	0.3	99.7	
V ETRIA-22	230	0.99	0.08	10.76	12.64	−0.32	0.13	4.41	8.45	793	0.39	3.1	96.9	1.03	0.061	1.4	98.6	−0.13
V ETRIA-23	245	1.02	0.09	2.18	2.51			3.31	3.35	422	0.21	8.3	91.7	1.12	0.013	0.4	99.6	
V ETRIA-24	250	1.00	0.14	4.72	5.51			2.47	1.11	878	0.43	7.8	92.2	1.09	0.009	0.4	99.6	
V ETRIA-25	255	0.92	0.12	4.50	5.15	−0.29	0.11	3.48	3.05	1035	0.51	11.3	90.1	1.04	0.029	0.8	99.2	
V ETRIA-26	270	1.09	0.06	2.68	3.25			2.28	1.99	137	0.07	2.1	97.9	1.11	0.002	0.1	99.9	
V ETRIA-27	280	0.89	0.12	6.83	7.33			1.50		176	0.09	1.2	98.8	0.90				
V ETRIA-28	290	0.67	0.09	1.85	2.15	−0.41	0.07	4.80	3.17	1048	0.51	23.9	76.1	0.92	0.030	0.6	99.4	−0.21
V ETRIA-29	300	0.83	0.05	2.48	3.19			3.60	3.41	1019	0.50	15.7	84.3	1.01	0.032	0.9	99.1	
V ETRIA-30	315	0.80	0.09	3.96	4.79	−0.29	0.05	1.15	0.75	663	0.33	6.8	93.2	0.87	0.004	0.4	99.6	−0.10
V ETRIA-31	325	0.89	0.10	2.81	3.36	−0.43	0.06	6.63	7.12	183	0.09	2.7	97.3	0.92	0.012	0.2	99.8	−0.23
Average		0.86		4.27	5.25	−0.34		3.79	3.85			6.8	93.2	0.93	0.021	0.5	99.5	-0.14
2 σ		0.12		2.62	3.72	0.07		3.62	4.24			10.3	10.3	0.24	0.017	0.7	0.7	0.15

ICP = Inductively Coupled Plasma; det = detrital; auth = authigenic; ID = Isotope Dilution.

concentrations ([Cr_{det}]), and detrital and authigenic Cr fractions (% Cr_{det}; %Cr_{auth}) are also listed in Table 1. The low %Cr_{det} fractions (range between 2.7 and 23.9%) enabled the calculation of fairly solid $\delta^{53}Cr_{auth}$ values. These are relatively homogeneous and define an average $\delta^{53}Cr_{auth}$ value of +0.93 ± 0.24 ‰ (2σ, $n = 30$; Table 1; Fig. 4).

3.5. Cd-isotopes

Table 1 lists the [Cd] and δ^{114}Cd values of those mesoband samples which we could successfully analyze. As mentioned before, the very low [Cd] in the hematite mesobands (average of 3.8 ± 2.4 ng/g; 2σ, $n = 24$) posed an analytical challenge, mainly related to the ion chromatographic removal of the very large Fe matrices. The insensitivity towards siliciclastic contamination (detrital [Cd] shares listed in Table 1 are <1.4% relative to total [Cd]; calculations analogous to eqs. 7–9 for [Cr] using [Cd] of average loess of 0.12 μg/g and a δ^{114}Cd value of +0.08‰ reported by Schmitt et al. (2009) for the correction routines) of measured δ^{114}Cd made it unnecessary to perform detrital share corrections (since these only affect the third digit of the δ^{114}Cd values; Table 1). The measured δ^{114}Cd values are therefore considered to be essentially authigenic in nature. Similar to δ^{53}Cr values, δ^{114}Cd values are quite homogenously distributed along the studied core profile (Fig. 4) and define a narrow range between −0.23 and + 0.01 ‰, with an average of −0.14 ± 0.14 ‰ (2σ; $n = 15$) (Table 1). In particular, there is no difference between δ^{114}Cd values of hematite mesobands from the upper, cherty/jaspilitic part to the Banda Alta Formation, and mesoband samples from the lower carbonatic part, possibly pointing to carbonates being a less important Cd host compared to hematite.

4. Discussion

4.1. Major element properties

Bulk core sample compositions differ significantly from the hematite mesoband samples, as expected with respect to [Fe] and [Si], but also with respect to major elements [Al] and [Ca] which are indicative of siliclastic components and carbonate minerals. The low [Ca] and [Al] in the mesobands indicates that we were successful in separating pure hematite bands from both carbonatic and cherty/jaspilitic IF sequences, and that we efficiently circumvented mesobands with detrital siliciclastic components (hematite mesoband samples studied herein contain only small amounts of [Al] typically <~1000 mg/Kg; Table 1). The divergence in Mg + Ca between the outcrop samples from Morro Urucum (Frei et al., 2017) and drill core mesoband samples studied herein from Morro Grande (Table A1) can be explained as the result of either a lack of sampling of carbonatic IF by Frei et al. (2017), or more likely, as a consequence stemming from the leaching of carbonate minerals in the surface samples as a result of weathering.

4.2. REY patterns and water sources

Positive Eu-anomalies in seawater correlate with the contribution of high-temperature hydrothermal fluid input to the oceans (Elderfield et al., 1997; German et al., 1990). Archean and Proterozoic BIFs are characterized by positive Eu anomalies in their REY patterns, and therefore this is traditionally interpreted to signify the admixture of high-temperature fluids to continentally derived solutes entering the oceans via run-off (Derry and Jacobsen, 1990; Dymek and Klein, 1988).

The hematite mesoband samples studied herein do not exhibit positive Eu-anomalies in their REY patterns (Eu/Eu* = 1.02 +/− 0.08 (2σ, $n = 30$; Fig. 5A; Table A1). The similar lack of positive Eu-anomalies in the Cryogenian glaciogenic Rapitan IF has been explained by (1) inhibition of long-distance transport of hydrothermally derived Eu(II) as a results of sufficiently oxidized open ocean waters (Baldwin et al., 2012), and/or by (2) an effective isolation of depositional basins from the open oceans (Klein and Beukes, 1993). Explanation (2) is compatible with rift-graben tectonic models for the depositional environment of the Jacadigo Group put forward by Freitas et al. (2021), Graf et al. (1994) and Urban et al. (1992). According to Frei et al. (2017), however, this model does not account for the source for the large quantities of Fe and Mn, and the different REY patterns observed by many research groups (Angerer et al., 2016; Frei et al., 2017; Graf et al., 1994; Klein and Ladeira, 2004; Viehmann et al., 2016) for IFs from the Urucum district. Furthermore, while it tentatively could explain a potential low-T hydrothermal fluid- and/or freshwater input to the surface waters (similar to what has been proposed for the source of Fe and Mn in the ca. 2.4 Ga Hotazel Formation; Schier et al., 2020), postulated by Freitas et al. (2021) and Walde et al. (2015), it does not conform with the transition to the open shelf setting of the Corumbá Group carbonates overlying the IFs of the Banda Alta Formation (Gaucher et al., 2003).

Similar to the Neoproterozoic Rapitan IF (Baldwin et al., 2012; Halverson et al., 2011), Early Cambrian IFs from the Jiertieke, Yelike, and Taaxi regions in Western China (Liang et al., 2006) also lack positive Eu-anomalies in their REY patterns and therefore contradict a high-temperature fluid scenario for the source of Fe in these deposits. A low-temperature scenario, on the other hand, and as mentioned above, would be in line with the *syn*-tectonic depositional model for the Corumbá graben (Freitas et al., 2011). Such a scenario would allow a deep-water metal fertilization of the Jacadigo Basin as argued for by Angerer et al. (2016), Frei et al. (2017), Viehmann et al. (2016) and Walde and Hagemann (2007). Our new REY patterns of pure hematite mesobands from Morro Grande partially resemble those published by Árting et al. (2023), and they are also similar to REY patterns of pure IF samples from both Morro Urucum and Morro Rabichão reported by Viehmann et al. (2016) and Angerer et al. (2016). The REY patterns of iron-rich mesobands presented herein are typically seawater-like throughout the entire Banda Alta Formation. They are characteristically positively sloped, exhibit predominantly negative Ce/Ce* and show positive Y/Ho anomalies (Fig. 5A, B). If we compare our new REY patterns with those published by Angerer et al. (2016) for the Santa Cruz deposit on Morro Grande, we notice that all of them pertain to type (I) patterns (classified as seawater-like patterns) categorized by these authors. None of the other patterns observed by Angerer et al. (2016) (i.e., type (II) patterns characterized by positive slopes with only small negative Ce/Ce*; and type (III) patterns characterized by flat slopes with slightly MREE enriched (humped) buckles) are represented by our samples. We attribute this to the pureness of the hematite mesoband samples prepared for analyses in this study. We also note that REY patterns from hematite mesobands from within the upper, cherty/jaspilitic, and from the lower carbonatic Banda Alta Formation section cannot be distinguished from each other in their pattern shapes (cf., Fig. 5A), despite the difference in carbonate content of the mesobands. Ca-carbonates could potentially contribute with LREE and MREE to the overall REY budgets. The lack of significant covariance of Ca with ∑REE and Pr/Yb in the IF samples studied by Angerer et al. (2016), also in the hematite mesobands studied herein (Table A1; not plotted here), suggests that Ca-carbonates are not major contributors to the REE budget of the hematite mesobands.

Positive Ce anomalies in suspended particulate phases of modern oceans (and likewise the presence of correspondingly negative Ce anomalies in oxidized seawater) haves been interpreted to derive from adsorption of REE(III)s onto particulate MnO_2 surfaces, subsequent oxidation of Ce(III) to Ce(IV) at shallow depths, and following preferential release of the light REEs over Ce(IV) at deeper depths by desorption (Alibo and Nozaki, 1999; Tachikawa et al., 1997). Negative Ce anomalies in marine chemical sediments are therefore regarded to reflect deposition from oxidized water columns. The seawater-like REY patterns observed for hematite mesoband samples from Morro Grande studied herein, for most mesobands studied by Árting et al. (2023), and for those pure bulk IF samples from Morro Rabichão and from Morro Urucum studied by Viehmann et al. (2016), are compatible with deposition from a water column characterized, at least periodically, by the

presence of an oxidized surface water layer.

4.3. Redox sensitive trace elements

Mo and U exhibit a similar behavior in aqueous solution. Both elements are soluble as Mo(VI) and U(VI) under oxic conditions and exhibit conservative behavior with long residence time, as observed in modern seawater. They become particle reactive under anoxic conditions, as they are consequently removed from the water column through adsorption onto Fe-sulfides, Fe and Mn oxides, organic matter and clays (Algeo and Tribovillard, 2009). In case of IFs, in the absence of euxinic conditions, U(VI) and Mo(VI) is removed from the water column by sorption onto iron oxyhydroxides in form of particle reactive uranyl carbonate and molybdate ions. In this the removal pathway resembles that of Cr(VI), where iron oxyhydroxides act as strong reducers for Cr (VI) in a coupled reaction, producing highly particle reactive Cr(III). If Fe^{2+} is in surplus, Cr is quantitatively stripped from the seawater according to the reaction 3 Fe(II) + Cr(VI) → 3 Fe(III) + Cr(III) preferred as mechanism to explain the Cr isotope record in BIFs through time (Frei et al., 2009). Effective and rapid stripping of dissolved Cr(VI) in this way renders the residence time for Cr very short and enables therefore short time scale resolution studies in IF depositional basins. Mildly euxinic conditions are required for Mo to become particle reactive, while U is reactive regardless of sulfidic species (Algeo and Tribovillard, 2009; Morford and Emerson, 1999). This different behavior likely leads to differentiated relative enrichments in respective sediments, and this feature can be used to further infer redox conditions in the basin. Uranium accumulation exceeds that of Mo in sediments formed in present-day open oceans with oxic bottom waters. In contrast, Mo is preferentially scavenged in euxinic basins, and this causes a shift to higher U/Mo ratios in respective basin waters (Algeo and Tribovillard, 2009).

In the context of the U—Mo relationships in present-day seawater described by Algeo and Tribovillard (2009), the Jacadigo Basin was likely a partially restricted basin similar to the modern Cariaco Basin. In such a basin, bounded by a bathymetric high, partial mixing of basin surface waters with the open ocean water is possible, while mixing between surface and bottom waters would be likely inhibited (Lyons et al., 2003). In fact, the bathymetric high allows the Cariaco Basin to sustain a separate redoxcline from the open oxygenated ocean, allowing even euxinic conditions to develop in the bottom waters. The maintenance of a steady supply of Mo from the open ocean in such a scenario would develop a steep Mo-enriched pattern in U_{EF}-Mo_{EF} space (Fig. 6A). In case such a basin closes off, the Mo supply from the open ocean would be inhibited and Mo would be stripped efficiently under developing euxinic conditions. The basin waters then would show a relative increase in U_{EF}, which would be expressed by horizontal deviation trends from the seawater trend line in the U_{EF}-Mo_{EF} diagram of Fig. 6A. The data computed herein for the hematite mesobands imply a partially restricted nature of the Jacadigo Basin as indicated by some data points in U_{EF}-Mo_{EF} space (Fig. 6A). Periods where the basin was likely fully silled are also indicated by relative enrichments of U with data points plotting in near-horizontal trends in Fig. 6A, potentially reflecting the development of euxinic bottom water conditions. Such conditions are particularly constrained to the carbonatic lower Banda Alta formation, i.e. to the earlier period of iron formation deposition. The existence of such conditions has been inferred by previous studies on the basis of varying REY patterns (Angerer et al., 2016; Árting et al., 2023; Frei et al., 2017; Freitas et al., 2011) in IFs from the Urucum district.

The intermittent relative U enrichment that is shown by many of our samples (Fig. 6A) suggests that the basin was sporadically connected to the open ocean, allowing oxic/suboxic conditions to develop in periods where the Jacadigo Basin had limited exchange with oxygenated ocean surface water. This was probably the case during periods of glacier advance stages which prevented the surface waters from being in contact with the oxygenated atmosphere.

4.4. Cr-isotope signal

Quantitative removal of Cr from the surface water is a valid scenario in the case of the Jacadigo Basin. It has already been suggested by Árting et al. (2023) and Frei et al. (2017), who argued that a constant supply of Fe^{2+} from anoxic, ferruginous bottom waters below a redoxcline would likely allow an efficient reductive removal of isotopically heavy Cr(VI), as well as Mo and U from oxic surface waters. Assuming surplus dissolved Fe^{2+} fertilized surface water conditions, the homogenous Cr isotope record in hematite mesobands throughout the Banda Alta Formation also entails that there were no significant changes in particulate Cr isotope composition during transport from surface water to the anoxic bottom waters. Thus, the reduced, isotopically heavy Cr(III) incorporated in the iron rich sediments likely records the isotope composition of dissolved Cr in the ambient surface seawater of the Jacadigo Basin. Cr isotopes in iron-rich chemical sediments may potentially directly record a mixture of four different Cr input sources into the basin. These are: (1) direct riverine input to the basin, i.e. in the case of the Jacadigo Basin, runoff from the Rio Apa Block; (2) if applicable, any subaqueous high-temperature hydrothermal input to the basin; (3) contribution of Cr from the open ocean; and (4) input from glacially-sourced Cr, included in iron oxyhydroxides that were bacterially reduced to dissolved ferrous iron.

Scenario (4) was favored by Baldwin et al. (2012) for the genesis of the Rapitan IF. These authors postulated that strong primary productivity in the shallow water column would be necessary to establish a three-tiered stratified water column with ferruginous deep water, an oxic surface water layer forming during glacier retreat stages, and an euxinic wedge at middle depths forming as a consequence of extreme shallow water primary productivity and eutrophication. High primary productivity in the surface waters of the Jacadigo Basin, as discussed below, can be refuted by the Cd isotope signatures recorded in the hematite mesobands.

Cr input scenario (3) would have only been possible in periods during which an open exchange between the Jacadigo Basin and the open ocean was established, and it would be recorded in relative Mo enrichment over U, with data expected to scatter around the Mo/U_{SW} trend line in Fig. 6A. If Cr was essentially sourced in the open ocean, one would expect to see some correlation with Mo and U (not considering the potential establishment of euxinic conditions during certain time periods). This is not demonstrated by our data set presented herein, and we prefer to interpret this to indicate a decoupling of Mo and U from Cr as a consequence of their different residence times.

This leaves us with the first two scenarios (scenario (1) and (2) referred to above) for potential sources of Fe and Cr in the Jacadigo Basin. The lack of positive Eu anomalies in the REY patterns of the mesobands speaks against involvement of high-T hydrothermal fluids (scenario (2)) in the Jacadigo Basin.

A mixing between a fresh-water and seawater (as implied by scenario (1)) would potentially be recorded by variations in the slope of REY patterns and by suppressed Y/Ho ratios. Instead, the patterns plotted in Fig. 5A are sub-parallel and only distinguished by their inferred total REY contents (cf. Table A1), a feature contesting a priori against a local freshwater-ocean water mixing scenario, although freshwater input during glacial meltdown certainly must have been a realistic scenario. In this case, if such mixing in fact did take place, then the freshwater component must have been low in overall metal (nutrient) concentrations (such as potentially would be expected for glacier melt waters).

Although a low-temperature hydrothermal contribution cannot be excluded completely, it leaves open ocean surface water (and ultimately land-sourced and river-transported input of Cr(VI)) as the most likely source for positively fractionated Cr isotopes in the Jacadigo Basin.

Other late Neoproterozoic IFs also show positively fractionated $\delta^{53}Cr$ values. Examples are: Arroyo del Soldado (Cerro Espuelitas Fm.) Fe-cherts, Uruguay, $\delta^{53}Cr_{mean}$ + 1.3 ‰, ca. 0.55 Ga; Yerbal IF, Uruguay, $\delta^{53}Cr_{mean}$ + 1.5 ‰, ca. 0.57 Ga; Rapitan IF, Canada, $\delta^{53}Cr_{mean}$ + 0.9 ‰,

0.7 Ga (all from (Frei et al., 2009)); the Chuos and Jakalsberg IF, Namibia, $\delta^{53}Cr_{mean}$ + 0.7 ‰ and + 0.8 ‰, respectively, 0.73 and 0.63 Ga respectively (Frei et al., 2017); Xiajiajiang IF (Fulu Formation), South China, average $\delta^{53}Cr$ + 0.91‰ (Wei et al., 2018c).

4.5. Cr-isotope composition of Jacadigo Basin surface seawater

The $\delta^{53}Cr_{auth}$ values recorded by the hematite mesoband studied herein are in agreement with $\delta^{53}Cr$ values of +0.13–1.53 ‰ of modern day surface seawater (Bonnand et al., 2013; Bruggmann et al., 2019b; Farkaš et al., 2018; Goring-Harford et al., 2020; Goring-Harford et al., 2018; Janssen et al., 2020; Paulukat et al., 2016; Pereira et al., 2015; Rickli et al., 2019; Scheiderich et al., 2015).

Biogenic fractionation of Cr isotopes plays a major role in Cr cycling in the modern ocean as recently shown (Janssen et al., 2020; Rickli et al., 2019; Semeniuk et al., 2016). Another study by Janssen et al. (2022) on the water column of the redox-stratified Lake Cadagno (Switzerland), which is considered a modern Proterozoic ocean analog, challenges quantitative Cr reduction scenarios in paleoredox reconstructions of water $\delta^{53}Cr$. As shown by these authors, non-quantitative Cr removal can lead to sediment $\delta^{53}Cr$ that are different from dissolved Cr isotope signatures in the overlying waters, and as demonstrated for Lake Cadagno, do not reflect high $\delta^{53}Cr$ from oxidative continental weathering. Janssen and co-workers (Janssen et al., 2022) show that removal of isotopically light Cr produced by biogenic reduction of Cr either directly or through production of Cr reductants, e.g. Fe^{2+}, explains isotopically light Cr(III) signals in sediments deposited in the deep ocean, and offers an alternative scenario for isotopically heavy dissolved Cr(VI) fractions in the surface layers. Non-quantitative Cr removal above the chemocline (in which ~20–60% of [Cr] in the surface water is commonly reduced; Janssen et al., 2022), enables the transport and accumulation of isotopically light $\delta^{53}Cr$ to anoxic deep waters, as demonstrated by these authors for Lake Cadagno, from where Cr is poorly sequestered into sediments. The Lake Cadagno study led them therefore to excerpt concerns for reconstructions of surface water columns or weathering conditions from $\delta^{53}Cr$ signals from sediments deposited in these environments. In their view, such reconstructions require accounting for fractionation during Cr removal as well as internal water column cycling which would result in variable water column $\delta^{53}Cr$.

If non-quantitative biogenic Cr reduction was the primary control on $\delta^{53}Cr$ in the Jacadigo Basin, it would require a complementary reservoir characterized by isotopically light(er) Cr. Organic-rich particulate matter would offer one possibility, but the chemical sediments of the Banda Alta Formation are devoid of organic matter. Remineralization of potentially formed organic particles carrying light Cr isotopes would, upon adsorption, impart heterogeneous isotope signatures in the settling iron oxyhydroxide particulate shuttle which then would be imparted in the hematite mesobands. This is obviously not the case as the latter are characterized by rather homogeneous $\delta^{53}Cr$ values (cf., Fig. 3; Table 1). We therefore deem it more likely that quantitative abiogenic Cr reduction was the predominant process for shuttling Cr from the surface waters to the sedimentary environment in the Jacadigo Basin. Such a scenario would be more realistic as it takes the efficiency of Cr reduction by the Fe(III) shuttle and the fact that large amounts of dissolved Fe(II) would have been required for IF deposition, into consideration. This does not a priori preclude bioproductivity (presence of phytoplankton) in the photic layer of the Jacadigo Basin, which may or may not have driven dissolved Cr in the surface water even more positively fractionated before its scavenging and stripping by iron oxyhydroxides upon upwelling of Fe^{2+} into the oxic surface waters. However, as discussed below, based on the Cd isotope record, we deem the primary production in the Jacadigo Basin surface waters to have been low, and consequently, the magnification of the isotopically heavy Cr signal from the runoff to even more positively fractionated $\delta^{53}Cr$ signatures was probably minimal.

The homogenous and strongly positively fractionated $\delta^{53}Cr$ signatures of hematite mesobands from the ca. 350 m-thick massive IF section at Morro Grande speak for a steady-state and effectively quantitative, Cr-exhaustive Fe^{2+} fertilization and removal from the Jacadigo Basin surface waters during the entire depositional period. Based on the above, we prefer to interpret the authigenic $\delta^{53}Cr$ values of hematite mesobands analyzed herein to closely reflect the average Cr isotope signature of the ambient surface water in the Jacadigo Basin during the IF depositional period.

4.6. Cd-isotopes

Similar to the Cr isotope records along the stratigraphic profile covered by the drill core studied herein, Cd isotope signatures are surprisingly homogeneous and define a narrow average $\delta^{114}Cd = -0.14 \pm 0.14$ (2σ; $n = 15$; Table 1, Fig. 3).

Iron oxyhydroxides can sequester Cd via adsorption and isomorphous substitution. In adsorption and co-precipitation experiments, Yan et al. (2021) recently showed that adsorption preferentially enriches lighter Cd isotopes on iron oxyhydroxide surfaces through equilibrium fractionation, with a similar fractionation magnitude ($\Delta^{114}Cd_{solid\text{-}solution}$) for goethite (Goe) (−0.51 ± 0.04‰), hematite (Hem) (−0.54 ± 0.10‰), and ferrihydrite (Fh) (−0.55 ± 0.03‰). In contrast, Cd incorporation into Goe by substitution for lattice Fe has shown to preferentially sequester heavy Cd isotopes, with a $\Delta^{114}Cd_{solid\text{-}solution}$ of 0.22 ± 0.01‰ (Yan et al., 2021). The fractionation has been proposed to probably occur during the transformation of Fh into Goe via dissolution and reprecipitation. The magnitude of these fractionations also has shown by these authors not to be influenced by either the initial Cd^{2+} concentration or ionic strength nor the pH.

The predominance of hematite in the mesoband samples studied, combined with the apparent lack of correlation between [Fe] and [Cd], attests for a massive predominance of dissolved Fe^{2+} over for dissolved Cd^{2+} which upon oxidation, potentially enabled efficient and quantitative removal of Cd from the surface waters in the Jacadigo Basin during periods of glacier retreats which allowed for exposure of the basin to the atmosphere. This would render the application of fractionation factors unnecessary as it would imply a quantitative transfer of the solution Cd isotope signature into the IF-precursor phases.

The lack of organic material (OM) in the Urucum IFs, and in particular in the hematite mesobands studied herein, does not preclude the existence of primary productivity (phytoplankton booms) in the surface waters of the Jacadigo Basin during exposure of the water masses to the atmosphere upon glacier retreat stages. Anaerobic OM remineralization by Fe(III) bearing phases (such as iron oxyhydroxides) is a known process (Boyd et al., 2010; Chen et al., 2022) and others. If, hypothetically, we assume that phytoplankton was present excessively during IF depositional periods, then this would have had a significant impact on the isotope signature of dissolved Cd in the surface waters. As in modern oceans, these waters likely would then have been characterized by positively fractionated $\delta^{114}Cd$ values, because of the fact that light Cd isotopes are preferably taken up by phytoplankton. If remaining dissolved Cd then would have been adsorbed onto iron oxyhydroxides in periods of upwelling Fe^{2+}-rich bottom waters, then the iron oxyhydroxide particle flux would have inherited these signatures, eventually leading to heterogeneously distributed $\delta^{114}Cd$ values in the iron-rich mesobands. The fact that the $\delta^{114}Cd$ values are relatively homogeneous and not positively fractionated, potentially signifies that primary productivity was low and that dissolved Fe^{2+} was in surplus over Cd^{2+}. This, in our opinion, is corroborated by the very low [Cd] in the mesobands.

Although Cd has experimentally shown to be adsorbed onto- or coprecipitated with iron oxyhydroxides with equilibrium isotope fractionation factors of ~ − 0.55 ‰ and ~ +0.22 ‰, respectively (Yan et al., 2021), our preferred scenario of a quantitative removal of Cd by surplus Fe^{2+} fertilization in the surfaces waters of the Jacadigo Basin would

favor a complete transfer of dissolved Cd from the solution to the solid IF precursor phase. In support of such a mechanism, experiments by Wasylenki et al. (2014) on Cd adsorption onto Fe—Mn hydroxides showed almost negligible fractionation the longer fluid and solid interacted with each other. In a complication of this scenario, assuming anaerobic remineralization of small amounts of potentially present OM by reduction of Fe(III) (flocculating iron oxyhydroxides), the isotopically light Cd that would have been associated with sinking OM, potentially would have been released into the deeper water and most likely adsorbed onto the iron oxyhydroxide particles. If operative, such a process would then have led to a shift towards somewhat lighter Cd isotope signatures in the settling iron oxyhydroxides. Such a scenario could in fact explain the slightly negatively fractionated Cd isotope signatures with an average δ^{114}Cd of −0.14 ± 0.14 (2σ; n = 15) we measured in the hematite mesobands.

In summary, we distinguish two scenarios: 1) a simple scenario in which phytoplankton control of the dissolved Cd in surface waters is neglected, and 2) a scenario in which both phytoplankton and iron oxyhydroxides impacted on the Cd inventory of the water column. In the first scenario, a surplus fertilization of the surface water columns with dissolved, upwelled Fe^{2+} would almost certainly remove the dissolved Cd completely, or quantitatively, similar to a nutrient supply-demand balanced consumption of Cd by primary producers and subsequent incorporation into sulfides forming in micro-environments of degrading/remineralizing OM under euxinic deeper water conditions (Georgiev et al., 2015; Sweere et al., 2020; Wang et al., 2023). In this respect, the δ^{114}Cd measured in the hematite mesobands would reflect the Cd isotope composition in the surface basin waters at times of glacier retreat stages and Fe^{2+}upwelling. In scenario two, in nutrient underbalanced situations, uptake of light Cd isotopes into primary producers would render surface water Cd isotopically heavy, and upon subsequent quantitative stripping by iron oxyhydroxides, this isotopically heavy signal would then be imparted into the IFs. Upon potential OM remineralization deeper down in the water column, portions of the isotopically light Cd associated with OM could eventually be transferred to and adsorbed by sinking iron oxyhydroxide particles, rendering these overall isotopically lighter. Reconstruction of the upper surface water layer composition would consequently underestimate the magnitude of ambient, positively fractionated Cd signatures therein, i.e., the iron oxyhydroxide signal attained from the surface water would be isotopically lowered, which would consequently result in the reconstruction of an isotopically too light δ^{114}Cd value in the surface water layer. At this stage we are unable to further elaborate on potential scenarios, but because of lack of indicators for a truly euxinic depositional environment (OM in the sediments, sulfides in the IFs), we prefer the simple scenario of a stratified basin with an anoxic deep water depositional environment and an oxic surface water layer in which bioproductivity was low during interglacial periods. Sulphur-undersaturated Neoproterozoic seawater with low sulphate-reducing bacteria activity, has for example been discussed as a result of the lack of typically sulphate-rich freshwater supply during glaciation (Hoffman, 2009; Swanson-Hysell et al., 2010). Alternatively, light Cd isotopic compositions in Neoproterozoic Cap Carbonates have also been explained by sulphate reduction in a stratified basin (Hohl et al., 2017).

Accepting the quantitative Cd stripping scenario by iron oxyhydroxides as preferential, then δ^{114}Cd signals in the mesobands (Table 1; Fig. 3) reflect the ambient Jacadigo Basin surface water signatures. These are significantly lower than those in modern ocean surface waters and potentially hint at very low primary production during severe glacial conditions. Carbon isotope values of pre- and post-glacial carbonates are typically negative (Halverson et al., 2002; Hoffman, 2009), near the canonical mantle value, suggesting that bioproductivity collapsed during the severe Neoproterozoic glaciations. Carbonates in the Banda Alta Formation yielded δ^{13}C values around −4 ‰ (Angerer et al., 2016), which agree well with a synglacial origin in a moment of low bioproductivity. This is especially surprising in the Jacadigo Basin, because upwelling of deep, anoxic water must have provided not only Fe but also other nutrients, such as P and N, which are more concentrated in deep ocean waters (De La Rocha, 2006). Moreover, biological diversity and prosperity likely flourished during post-snowball glaciation, particularly following the Marinoan glaciation. The atmospheric oxygen levels may have been sufficient to drive intense weathering and support biological survival (Bowyer et al., 2023; Krause et al., 2022). Upwelling systems are the most productive marine environments in the modern ocean (Kämpf and Chapman, 2016), and the same is assumed for ancient basins (e.g., Matheson et al. (2022)). The influx of meltwater from retreating glaciers, however, may have impaired the development of the biota by lowering salinity, as reported for present-day northern Baffin Bay (Bergeron and Tremblay, 2014). Finally, it is worth noting that Neoproterozoic glaciations were accompanied by the extinction of several taxa, although other species survived through the glacial events (Gaucher and Sprechmann, 2009; Moczydlowska, 2008). Neoproterozoic near-global glaciations were indeed challenging for the biota, and this may help explain the low bioproductivity recorded in the Jacadigo Basin. In any case, the perceived contradictions lined out above warrant further investigations in the future.

4.7. A depositional model for the Urucum IF

Angerer et al. (2016) argue for a *syn*-glacial model for the deposition of the Banda Alta Formation, with deposition of IFs during a transgression-regression cycle. These authors envisage a scenario based on systematic variations in REY patterns and δ^{57}Fe, in which the Jacadigo Basin is considered a marine sub-basin which received REY from freshwater, pore water or low-temperature hydrothermal sources, as well from open ocean waters. According to these authors, mixing of these different water sources led to three geochemically distinguishable iron formation facies.

In their study on drill-core samples from Morro Urucum and Morro Rabichão, Viehmann et al. (2016) found seawater-like REY patterns in pure iron formation which resemble those of the hematite mesobands analyzed in this study, besides shale-like patterns in IF samples with detrital siliciclastic contents.

The prevalence of seawater-like patterns in the central to upper part (200–30 m) of the drill-core samples analyzed by Árting et al. (2023) as well as sporadically elevated U_{EF}-Mo_{EF} reported by these authors from within the lower part of the core, support the transgressive model presented by Angerer et al. (2016) for the lower parts of the Banda Formation section. Increasing Y/Ho ratios in the mesobands studied herein (Fig. 5C) support this scenario. As argued by previous authors, connections of the Jacadigo Basin to open ocean likely were established during inter-glacial periods characterized by glacioeustatic sea-level rise (Árting et al., 2023; Frei et al., 2017; Viehmann et al., 2016).

Deposition of the IFs in the Jacadigo Basin exhibit pronounced similarities with the depositional environments proposed for the Cryogenian Rapitan IFs (Baldwin et al., 2012). Using redox sensitive element enrichment factors (Mo_{EF} and U_{EF}), and correlation diagrams of Mo vs. Fe_2O_3 and MnO, in which a strong relationship between these metals in an entirely oxic water column would be expected, Baldwin et al. (2012) postulated that Mo enrichment in the Raptian IFs happened under euxinic conditions instead. The lack of any strong correlation between Mo, Fe_2O_3 and MnO (not shown here), across the full range of hematite mesoband compositions presented herein, potentially signifies that Fe (and Mn) deposition rates were not a limiting factor in Mo enrichment, and that consequently a molybdate fixing particulate shuttle was not the sole scavenging mechanism to explain the Mo_{EF} in the Morro Grande IFs. Probably free H_2S, as proposed for the Rapitan IFs (Baldwin et al., 2012), was needed to drive Mo fixation instead, and this would then also explain the high U EF values in some of the hematite mesobands analyzed herein (Fig. 6A). The three samples with the strongest enrichment in U (samples VETRIA 21,23,26; Fig. 6A; Table A1) all are from within the lower, carbonatic Banda Alta Fm., and possibly

hint at periods of the basin evolution which likely were characterized by advanced glacier stages which prevented the surface waters to be in contact with the atmosphere.

The postulation of a redox-stratified Jacadigo Basin with anoxic bottom waters and with periods where a connection to open ocean waters was established, is otherwise corroborated by a comparison of Mo_{EF} vs. U_{EF} in the mesobands with the relationship of these elements in modern environmental scenarios (Fig. 6A). With the exception of those samples with strong U EF relative to Mo EF mentioned above, the scatter of data along the open marine trend in Fig. 6A and the proximity of the data to the seawater (Mo/U_{SW}) reference line would support such a connection of the Jacadigo Basin to open ocean waters. A broad connection of the upper parts of the water column with the open ocean allows for constant Mo supply. In connection with a slow exchange across the redoxcline, it allows for Mo enrichment over U, which is in part reflected by some of the hematite mesobands studied herein and by those of Árting et al. (2023) from the Urucum IF plotting above the 1:1 reference line in Fig. 6A. This is even more pronouncedly depicted by Urucum IF data of Viehmann et al. (2016), and by published data from Rapitan IFs (Baldwin et al., 2012); plotted in Fig. 6A for reference). These data sets mirror those exhibited in modern silled basin waters such as the Cariaco Basin (Algeo and Tribovillard, 2009).

All in all, it appears as if the Jacadigo Basin was characterized by fluctuating sea water levels and retreat/advance stages of glaciers which both had a strong impact on the water column structure and water column redox. For example, changes in sea level associated with glacial retreat are also consistent with the occurrence of Mn-beds in the lower Jacadigo Basin (Fig. 1). These were likely deposited in shallow, more oxic environments, on expanded shallow shelves during transgressive stages in the beginning of the depositional period of the Banda Alta Formation (Viehmann et al., 2016). The work of Viehmann et al. (2016) on Morro Rabichão and Morro Urucum, and the recent work by Árting et al. (2023) on hematite mesobands from Morro Grande, contrast with the study of Angerer et al. (2016), in that the latter authors find no evidence for significant freshwater influence. Rather, they consistently find seawater-like REY patterns like those depicted by the hematite mesobands studied herein, which are interpreted to imply open-ocean connection during interglacial periods. Viehmann et al. (2016) however recognized that the flat REY patterns observed in the Mn-horizons at the base of the Banda Alta Formation indicated a freshwater influx, and they proposed that these were in line with their model proposing shallow marine, more oxic shelf environments that prevailed during the beginning of the depositional period of the Banda Alta Formation. A similar model, namely the mixing and the involvement of low-temperature hydrothermal fluids and benthic fluxes of sediment pore waters transported by an upwelling current, followed by progressive partial oxidation of the fluid, was proposed by Huang et al. (2021) for constraining the metal source and depositional environment of the iron and manganese deposits in Urucum.

Taking all the trace-element and Cr-isotope data published on the Banda Alta Formation into consideration, and now also including the Cd isotope record presented herein, we then must conclude that the Jacadico Basin was a complex basin, most likely with several smaller sub-basins with locally varying redox conditions that were at times isolated from one-another. The surface layers of these sub-basins were periodically in contact with oxic ocean surface water, and these basins were fed and fertilized with nutrients and iron during periods of upwelling of anoxic deep water from the open ocean, in a scenario similar to that proposed for the ~600 Ma Algoma-type BIFs in the Seridó Group of northeastern Brazil by (Sial et al., 2015). Changing environmental conditions within the depositional realm of individual sub-basins are best reflected by the variability in Cr_{EF}, Mo_{EF} and U_{EF} presented here and in studies by Angerer et al. (2016), Frei et al. (2017), Viehmann et al. (2016), and most recently by Árting et al. (2023). Our Cd isotope record presented herein for the Banda Alta Formation IFs attests for depressed primary productivity and low nutrient supply during times of glacier retreats, despite the presence of continuously oxidized surface waters as implied by the strongly positively fractionated $\delta^{53}Cr_{auth}$ values in the hematite mesobands analyzed herein.

The seawater-like REY patterns of the hematite mesobands agree with the scenario of periodical connection of the Jacadigo sub-basins with the open ocean were the basins received their REY inventory and were fertilized by iron from upwelled anoxic deep ocean waters. Regardless of whether an open-marine signal was modified and/or diluted in the Jacadigo Basin by freshwater derived from glacier melt down, the lack of positive Eu-anomalies (Table A1; Fig. 5A) even in samples with the highest Y/Ho implies that the Neoproterozoic ocean appears to no longer had a prominent positive Eu anomaly derived from the input of high-temperature subaqueous fluids, as otherwise emphasized for BIFs of the Archean and Paleoproterozoic (e.g., Kato et al. (2006)). Signatures in the Cryogenian Rapitan IF (Baldwin et al., 2012) support this change in high-temperature fluid input to the open ocean, although some IF samples from the Jiertieke, Yelike, and Taaxi regions in Western China, found interlayered with metavolcanic rocks and classified as Algoma-type, revealed remarkably positive Eu anomalies pointing to sporadic influence of high-temperature hydrothermal fluids in certain depositional basins even in the Early Cambrian (Hu et al., 2020; Li et al., 2018).

The interpretation of the Banda Alta Formation as being deposited during a transgressional period is compliant with a deposition during glacial melting. The only small scatter of $\delta^{53}Cr_{auth}$ and $\delta^{114}Cd$ throughout the section and stratigraphically upward increasing Y/Ho ratios in the iron rich mesobands support this Jacadigo Basin evolution. Thin sea-ice, as in the model explaining the presence of rhytmites in the Cerradinho Formation overlying the Banda Alta Formation proposed by Hiatt et al. (2020), would have allowed an oxygenated surface layer to form, but a steady supply of Fe and sediment starvation (Freitas et al., 2011) would have kept iron oxyhydroxide formation the primary mode of precipitation throughout the Banda Alta Formation.

5. Conclusions

REY systematics, combined with varying redox-sensitive trace element (Cr, U and Mo) relationships in hematite mesobands of the Banda Alta Formation (Jacadigo Group) point to the presence of restricted sub-basins which periodically were connected to the open ocean and were fertilized with nutrients and iron by upwelled anoxic deep ocean waters. Isolation of the sub-basins from the open ocean was potentially established by ice sheets. Intermittent enrichment of U over Mo in the hematite mesobands of the Morro Grande drillcore studied herein suggests the occasional transformation of anoxic bottom layers of the stratified sub-basins to layers with euxinic water properties with the presence of free H_2S.

REY patterns of the mesobands are sub-parallel and seawater-like and have predominantly distinct negative Ce-anomalies but lack positive Eu-anomalies. If mixing of ocean surface water with freshwater from glacier meltdown did take place, then the freshwater must have been low in overall dissolved metal content. The inferred low metal content of an eventual freshwater component is compatible with very low Cd concentrations in the iron-rich mesobands, averaging 3.9 ± 2.2 ng/g.

Stratigraphically upward-increasing Y/Ho are compatible with a transgressive scenario for the deposition of the (particularly lower) Banda Alta Formation as proposed by Angerer et al. (2016).

Water mixing trends are not observed in $\delta^{53}Cr_{auth}$ and $\delta^{114}Cd$ values of the analyzed iron-rich mesobands which cover the entire thickness of the Banda Alta Formation. These non-traditional stable isotope signatures are rather homogeneously distributed over the entire stratigraphic profile and so imply relative stable surface water conditions, both with respect to redox and bioproductivity levels. Throughout strongly positively fractionated $\delta^{53}Cr_{auth}$ values averaging 0.93 ± 0.24 ‰ (2σ; n = 23) exhibited by the mesobands are interpreted to reflect the ambient

surface waters of the Jacadigo Basin and are compatible with modern ocean surface waters. Lack of positively fractionated δ^{114}Cd isotope signatures, which would point to primary productivity in the surface waters, is taken as supporting evidence that the positively fractionated Cr isotope values are the result of isotopically heavy Cr(VI) input to the basin via run-off from continental landmasses that were exposed to oxidative weathering during the late Neoproterozoic, rather than the result of dominant biogenic fractionation as the case in the modern ocean scenarios.

The unexpectedly low and rather homogenous δ^{114}Cd values (average of -0.14 ± 0.14 ‰; 2σ, $n = 15$) measured in the iron-rich mesobands are interpreted to mimic the Cd isotope signature in the ambient surface waters, as we emphasize a quantitative stripping through adsorption/coprecipitation onto/with iron oxyhydroxides formed by upwelling of Fe^{2+} into the oxidized surface water of the Jacadigo Basin. These values then would indicate a low primary productivity during the IF depositional period in the *syn*-glacial scenario, if they are to compare with modern oceans.

The non-traditional stable Cr—Cd isotope tracer applied to banded iron formations has the potential to be useful in the reconstruction of redox and bioproductivity in ancient depositional basins.

CRediT authorship contribution statement

Robert Frei: Writing – review & editing, Writing – original draft, Visualization, Validation, Supervision, Project administration, Methodology, Investigation, Funding acquisition, Formal analysis, Conceptualization. **Claudio Gaucher:** Writing – review & editing, Investigation. **Paulo César Boggiani:** Writing – review & editing, Investigation, Funding acquisition. **Jesper Allan Frederiksen:** Writing – review & editing, Investigation. **Samantha Renee Walker:** Writing – review & editing, Investigation. **Henrique Albuquerque Fernandes:** Writing – review & editing, Visualization, Investigation. **Fabricio Caxito:** Writing – review & editing, Investigation.

Declaration of competing interest

The authors declare that they have no known competing financial interests or personal relationships that could have appeared to influence the work reported in this paper.

Data availability

No data was used for the research described in the article.

Acknowledgments

We are thankful to Vectorial Ltd. for providing access to field sites and the drill core sheds and allowing sampling of core STCR-DD-36-32. In particular, we thank Raphael Henson, who provided guidance in the Vectorial mine and shared his knowledge. Toby Leeper, Toni Larsen, Cristina Nora Jensen de Olsen and Martin Heckscher helped with mass spectrometric analyses, ion chromatographic separations and sample preparations, respectively. Ware thankful for the detailed, constructive and insightful comments provided by four anonymous reviewers, and for streamlining suggestions by editor Vasileios Mavromatis. This research is financed by the Independent Research Fund Denmark (grant 1026-00001B to RF), and by CNPq (Proc 2014/01233-0) and FAPESP (Proc 2004/01233-0, Proc 2016/06114-6 and Proc 2020/16140-0) to PCB.

Appendix A. Supplementary data

Supplementary data to this article can be found online at https://doi.org/10.1016/j.chemgeo.2024.122101.

References

Abbey, S., McLeod, C., Wan, L.-G., 1983. FeR-1, FeR-2, FeR-3 and FeR-4, Four Canadian Iron-Formation Samples Prepared for Use as Reference Materials. Geological Survey of Canada.
Abouchami, W., Galer, S.J.G., de Baar, H.J.W., Alderkamp, A.C., Middag, R., Laan, P., Feldmann, H., Andreae, M.O., 2011. Modulation of the Southern Ocean cadmium isotope signature by ocean circulation and primary productivity. Earth Planet. Sci. Lett. 305, 83–91.
Abouchami, W., Galer, S.J.G., Horner, T.J., Rehkamper, M., Wombacher, F., Xue, Z.C., Lambelet, M., Gault-Ringold, M., Stirling, C.H., Schonbachler, M., Shiel, A.E., Weis, D., Holdship, P.F., 2013. A Common Reference Material for Cadmium Isotope Studies - NIST SRM 3108. Geostand. Geoanal. Res. 37, 5–17.
Abouchami, W., Galer, S.J.G., de Baar, H.J.W., Middag, R., Vance, D., Zhao, Y., Klunder, M., Mezger, K., Feldmann, H., Andreae, M.O., 2014. Biogeochemical cycling of cadmium isotopes in the Southern Ocean along the Zero Meridian. Geochim. Cosmochim. Acta 127, 348–367.
Algeo, T.J., Maynard, J.B., 2008. Trace-metal covariation as a guide to water-mass conditions in ancient anoxic marine environments. Geosphere 4, 872–887.
Algeo, T.J., Tribovillard, N., 2009. Environmental analysis of paleoceanographic systems based on molybdenum-uranium covariation. Chem. Geol. 268, 211–225.
Alibo, D.S., Nozaki, Y., 1999. Rare earth elements in seawater: Particle association, shale-normalization, and Ce oxidation. Geochim. Cosmochim. Acta 63, 363–372.
Allen, P.A., Etienne, J.L., 2008. Sedimentary challenge to Snowball Earth. Nat. Geosci. 1, 817–825.
Almeida, F.F.M., 1965. Geologia da Serra da Bodoquena (Mato Grosso), Brasil. Bol. Divisão Geol. Mineral. 219, 1–96.
Angerer, T., Hagemann, S.G., Walde, D.H.G., Halverson, G.P., 2016. Multiple metal sources in the glaciomarine facies of the Neoporterozoic Jacadigo iron formation in the "Santa Cruz deposti", Corumbá, Brazil. Precambrian Res. 275, 369–393.
Árting, T.B., Boggiani, P.C., Gaucher, C., Fernandes, H.A., Frei, R., 2023. Strong positive fractionation of chromium isotopes in iron formation of the Jacadigo Group (Brazil) – a link to enhanced atmospheric oxygenation during the late Neoproterozoic. Gondwana Res. 124, 39–60.
Babinski, M., Boggiani, P.C., Trindade, R.I.F., Fanning, C.M., 2013. Detrital zircon ages and geochronological constraints on the Neoproterozoic Puga diamictites and associated BIFs in the southern Paraguay Belt, Brazil. Gondwana Res. 23, 988–997.
Baldwin, G.J., Turner, E.C., Kamber, B.S., 2012. A new depositional model for glaciogenic Neoproterozoic iron formation: insights from the chemostratigraphy and basin configuration of the Rapitan iron formation. Can. J. Earth Sci. 49, 455–476.
Basta, F.F., Maurice, A.E., Fontboté, L., Favarger, P.-Y., 2011. Petrology and geochemistry of the banded iron formation (BIF) of Wadi Karim and Um Anab, Eastern Desert, Egypt: Implications for the origin of Neoproterozoic BIF. Precambrian Res. 187, 277–292.
Bau, M., 1999. Scavenging of dissolved yttrium and rare earths by precipitating iron oxyhydroxide: Experimental evidence for Ce oxidation, Y-Ho fractionation, and lanthanide tetrad effect. Geochim. Cosmochim. Acta 63, 67–77.
Bau, M., Dulski, P., 1996. Distribution of yttrium and rare-earth elements in the Penge and Kuruman iron-formations, Transvaal Supergroup, South Africa. Precambrian Res. 79, 37–55.
Bekker, A., Holland, H.D., Wang, P.L., Rumble, D., Stein, H.J., Hannah, J.L., Coetzee, L. L., Beukes, N.J., 2004. Dating the rise of atmospheric oxygen. Nature 427, 117–120.
Bekker, A., Slack, J.F., Planavsky, N., Krapez, B., Hofmann, A., Konhauser, K.O., Rouxel, O.J., 2010. Iron Formation: the Sedimentary product of a complex Interplay among Mantle, Tectonic, Oceanic, and Biospheric Processes. Econ. Geol. 105, 467–508.
Benjamin, M.M., Leckie, J.O., 1981a. Competitive adsorption of cd, cu, zn, and pb on amorphous iron oxyhydroxide. J. Colloid Interface Sci. 83, 410–419.
Benjamin, M.M., Leckie, J.O., 1981b. Multiple-site adsorption of Cd, Cu, Zn, and Pb on amorphous iron oxyhydroxide. J. Colloid Interface Sci. 79, 209–221.
Bergeron, M., Tremblay, J.-É., 2014. Shifts in biological productivity inferred from nutrient drawdown in the southern Beaufort Sea (2003−2011) and northern Baffin Bay (1997–2011), Canadian Arctic. Geophys. Res. Lett. 41, 3979–3987.
Beukes, N.J., Klein, C., 1990. Geochemistry and Sedimentology of a Facies transition - from Microbanded to Granular Iron-Formation - in the early Proterozoic Transvaal Supergroup, South Africa. Precambrian Res. 47, 99–139.
Beukes, N.J., Klein, C., 1992. Models for iron-formation deposition. In: Schopf, J.W., Klein, C. (Eds.), The Proterozoic Biosphere: A Multidisciplinary Study. Cambridge University Press, New York, pp. 147–151.
Bolhar, R., Kamber, B.S., Moorbath, S., Fedo, C.M., Whitehouse, M.J., 2004. Characterisation of early Archaean chemical sediments by trace element signatures. Earth Planet. Sci. Lett. 222, 43–60.
Bonnand, P., Parkinson, I.J., James, R.H., Karjalainen, A.-M., Fehr, M.A., 2011. Accurate and precise determination of stable Cr isotope compositions in carbonates by double spike MC-ICP-MS. J. Anal. At. Spectrom. 26, 528–536.
Bonnand, P., James, R.H., Parkinson, I.J., Connelly, D.P., Fairchild, I.J., 2013. The chromium isotopic composition of seawater and marine carbonates. Earth Planet. Sci. Lett. 382, 10–20.
Bowyer, F.T., Krause, A.J., Song, Y., Huang, K.-J., Fu, Y., Shen, B., Li, J., Zhu, X.-K., Kipp, M.A., van Maldegem, L.M., Brocks, J.J., Shields, G.A., Le Hir, G., Mills, B.J.W., Poulton, S.W., 2023. Biological diversification linked to environmental stabilization following the Sturtian Snowball glaciation. Sci. Adv. 9, eadf9999.
Boyd, P.W., Ibisanmi, E., Sander, S.G., Hunter, K.A., Jackson, G.A., 2010. Remineralization of upper ocean particles: Implications for iron biogeochemistry. Limnol. Oceanogr. 55, 1271–1288.

Boyle, E.A., 1988. Cadmium: Chemical tracer of Deepwater paleoceanography. Paleoceanography 3, 471–489.
Bridgestock, L., Rehkämper, M., van de Flierdt, T., Murphy, K., Khondoker, R., Baker, A. R., Chance, R., Strekopytov, S., Humphreys-Williams, E., Achterberg, E.P., 2017. The Cd isotope composition of atmospheric aerosols from the Tropical Atlantic Ocean. Geophys. Res. Lett. 44, 2932–2940.
Bruggmann, S., Klaebe, R.M., Paulukat, C., Frei, R., 2019a. Heterogeneity and incorporation of chromium isotopes in recent marine molluscs (Mytilus). Geobiology 17, 417–435.
Bruggmann, S., Scholz, F., Klaebe, R.M., Canfield, D.E., Frei, R., 2019b. Chromium isotope cycling in the water column and sediments of the Peruvian continental margin. Geochim. Cosmochim. Acta 257, 224–242.
Bryan, A.L., Dickson, A.J., Dowdall, F., Homoky, W.B., Porcelli, D., Henderson, G.M., 2021. Controls on the cadmium isotope composition of modern marine sediments. Earth Planet. Sci. Lett. 565, 116946.
Canfield, D.E., Poulton, S.W., Knoll, A.H., Narbonne, G.M., Ross, G., Goldberg, T., Strauss, H., 2008. Ferruginous conditions dominated later Neoproterozoic deep-water chemistry. Science 321, 949–952.
Chen, L., Little, S.H., Kreissig, K., Severmann, S., McManus, J., 2021. Isotopically Light Cd in Sediments Underlying Oxygen Deficient Zone, p. 9.
Chen, Z., Nie, T., Zhao, X., Li, J., Yang, B., Cui, D., Li, X., 2022. Organic carbon remineralization rate in global marine sediments: a review. Reg. Stud. Mar. Sci. 49, 102112.
Conway, T.M., John, S.G., 2015a. Biogeochemical cycling of cadmium isotopes along a high-resolution section through the North Atlantic Ocean. Geochim. Cosmochim. Acta 148, 269–283.
Conway, T.M., John, S.G., 2015b. The cycling of iron, zinc and cadmium in the North East Pacific Ocean - Insights from stable isotopes. Geochim. Cosmochim. Acta 164, 262–283.
Cowan, C.E., Zachara, J.M., Resch, C.T., 1991. Cadmium adsorption on iron oxides in the presence of alkaline-earth elements. Environ. Sci. Technol. 25, 437–446.
D'Arcy, J., Babechuk, M.G., Dossing, L.N., Gaucher, C., Frei, R., 2016. Processes controlling the chromium isotopic composition of river water: Constraints from basaltic river catchments. Geochim. Cosmochim. Acta 186, 296–315.
De La Rocha, C.L., 2006. The biological pump. In: Ed. (Ed.), Elderfield, H. Treatise on geochemistry, pp. 83–111.
Derry, L.A., Jacobsen, S.B., 1990. The chemical evolution of Precambrian seawater: evidence from REEs in banded iron formations. Geochim. Cosmochim. Acta 54, 2965–2977.
Døssing, L.N., Dideriksen, K., Stipp, S.L.S., Frei, R., 2011. Reduction of hexavalent chromium by ferrous iron: a process of chromium isotope fractionation and its relevance to natural environments. Chem. Geol. 285, 157–166.
Droser, M.L., Gehling, J.G., 2015. The advent of animals: the view from the Ediacaran. Proc. Natl. Acad. Sci. 112, 4865–4870.
Druce, M., Stirling, C.H., Bostock, H.C., Rolison, J.M., 2022. Cadmium isotope systematics in sedimentary carbonate: Extending the utility of the cadmium isotope palaeo-productivity proxy. Geochim. Cosmochim. Acta 339, 80–96.
Dymek, R.F., Klein, C., 1988. Chemistry, Petrology and Origin of Banded Iron-Formation Lithologies from the 3800-Ma Isua Supracrustal Belt, West Greenland. Precambrian Res. 39, 247–302.
Elderfield, H., Whitfield, M., Burton, J.D., Bacon, M.P., Liss, P.S., Charnock, H., Lovelock, J.E., Liss, P.S., Whitfield, M., 1997. The oceanic chemistry of the rare-earth elements. Philosophical transactions of the Royal Society of London. Series A, Mathemat. and Phys. Sci. 325, 105–126.
Eriksson, P.G., Altermann, W., Nelson, D.R., Mueller, W.U., Catuneanu, O., 2004. Chapter 5 - Evolution of the Hydrosphere and Atmosphere. In: Eriksson, P.G., Altermann, W., Nelson, D.R., Mueller, W.U., Catuneanu, O. (Eds.), Developments in Precambrian Geology. Elsevier, pp. 359–511.
Farkaš, J., Chrastný, V., Novák, M., Čadkova, E., Pašava, J., Chakrabarti, R., Jacobsen, S. B., Ackerman, L., Bullen, T.D., 2013. Chromium isotope variations (δ53/52Cr) in mantle-derived sources and their weathering products: Implications for environmental studies and the evolution of δ53/52Cr in the Earth's mantle over geologic time. Geochim. Cosmochim. Acta 123, 74–92.
Farkaš, J., Frýda, J., Paulukat, C., Hathorne, E., Matoušková, Š., Rohovec, J., Frýdová, B., Francová, M., Frei, R., 2018. Chromium isotope fractionation between modern seawater and biogenic carbonates from the Great Barrier Reef, Australia: Implications for the paleo-seawater δ53Cr reconstructions. Earth Planet. Sci. Lett. 498, 140–151.
Frederiksen, J.A., Klaebe, R.M., Farkaš, J., Swart, P.K., Frei, R., 2022a. Cadmium isotopes in Bahamas platform carbonates: a base for reconstruction of past surface water bioproductivity and their link with chromium isotopes. Sci. Total Environ. 806, 150565.
Frederiksen, J.A., Wei, W., Rugen, E.J., Ling, H.-F., Frei, R., 2022b. Cadmium isotopes in Late Ediacaran–Early Cambrian Yangtze Platform carbonates – Reconstruction of bioproductivity in ambient surface seawater. Palaeogeogr. Palaeoclimatol. Palaeoecol. 601, 111096.
Frederiksen, J.A., Thibault, N., Gilleaudeau, G.J., Bjerrum, C.J., Moreau, J., Frei, R., 2024. Combined cadmium and chromium isotopes record a collapse of bioproductivity across the Cretaceous—Paleogene boundary in the Danish basin. Chem. Geol. 654, 122058.
Frei, R., Gaucher, C., Poulton, S.W., Canfield, D.E., 2009. Fluctuations in Precambrian atmospheric oxygenation recorded by chromium isotopes. Nature 461, 250–253.
Frei, R., Gaucher, C., Dossing, L.N., Sial, A.N., 2011. Chromium isotopes in carbonates - a tracer for climate change and for reconstructing the redox state of ancient seawater. Earth Planet. Sci. Lett. 312, 114–125.
Frei, R., Poire, D., Frei, K.M., 2014. Weathering on land and transport of chromium to the ocean in a subtropical region (Misiones, NW Argentina): a chromium stable isotope perspective. Chem. Geol. 381, 110–124.
Frei, R., Crowe, S.A., Bau, M., Polat, A., Fowle, D.A., Dossing, L.N., 2016. Oxidative elemental cycling under the low O_2 Eoarchean atmosphere. Sci. Rep. 6, 21058.
Frei, R., Døssing, L.N., Gaucher, C., Boggiani, P.C., Frei, K.M., Bech Árting, T., Crowe, S. A., Freitas, B.T., 2017. Extensive oxidative weathering in the aftermath of a late Neoproterozoic glaciation – evidence from trace element and chromium isotope records in the Urucum district (Jacadigo Group) and Puga iron formations (Mato Grosso do Sul, Brazil). Gondwana Res. 49, 1–20.
Frei, R., Paulukat, C., Bruggmann, S., Klaebe, R.M., 2018. A systematic look at chromium isotopes in modern shells – implications for paleo-environmental reconstructions. Biogeosciences 15, 4905–4922.
Frei, R., Lehmann, B., Xu, L., Frederiksen, J.A., 2020. Surface water oxygenation and bioproductivity – a link provided by combined chromium and cadmium isotopes in early Cambrian metalliferous black shales (Nanhua Basin, South China). Chem. Geol. 552, 119785.
Frei, R., Xu, L., Frederiksen, J.A., Lehmann, B., 2021. Signals of combined chromium–cadmium isotopes in basin waters of the early Cambrian – results from the Maoshi and Zhijin sections, Yangtze Platform, South China. Chem. Geol. 563, 120061.
Freitas, B.T., Warren, L.V., Boggiani, P.C., De Almeida, R.P., Piacentini, T., 2011. Tectono-sedimentary evolution of the Neoproterozoic BIF-bearing Jacadigo Group, SW-Brazil. Sediment. Geol. 238, 48–70.
Freitas, B.T., Rudnitzki, I.D., Morais, L., Campos, M.D.R., Almeida, R.P., Warren, L.V., Boggiani, P.C., Caetano-Filho, S., Bedoya-Rueda, C., Babinski, M., Fairchild, T.R., Trindade, R.I.F., 2021. Cryogenian glaciostatic and eustatic fluctuations and massive Marinoan-related deposition of Fe and Mn in the Urucum District, Brazil. Geology 49, 1478–1483.
Gaucher, C., Sprechmann, P., 2009. Chapter 9.1 Neoproterozoic Acritarch Evolution. In: Gaucher, C., Sial, A.N., Frimmel, H.E., Halverson, G.P. (Eds.), Developments in Precambrian Geology. Elsevier, pp. 319–326.
Gaucher, C., Boggiani, P.C., Sprechmann, P., Sial, A.N., Fairchild, T., 2003. Integrated correlation of the Vendian to Cambrian Arroyo del Soldado and Corumba groups (Uruguay and Brazil): palaeogeographic, palaeoclimatic and palaeobiologic implications. Precambrian Res. 120, 241–278.
Gaucher, C., Sial, A.N., Frei, R., 2015. Chapter 17 - Chemostratigraphy of Neoproterozoic Banded Iron Formation (BIF): Types, Age and Origin. In: Ramkumar, M. (Ed.), Chemostratigraphy. Elsevier, Oxford, pp. 433–449.
Gault-Ringold, M., 2011. The Marine Biogeochemistry of Cadmium - Studies of Cadmium Isotopic Variations in the Southern Ocean. University of Otago, Dunedin, New Zealand, p. 125.
Georgiev, S.V., Horner, T.J., Stein, H.J., Bingen, B., Rehkamper, M., 2015. Cadmium-isotopic evidence for increasing primary productivity during the late Permian anoxic event. Earth Planet. Sci. Lett. 410, 84–96.
German, C.R., Klinkhammer, G.P., Edmond, J.M., Mitra, A., Elderfield, H., 1990. Hydrothermal Scavenging of Rare-Earth elements in the Ocean. Nature 345, 516–518.
Gerstenberger, H., Haase, G., 1997. A highly effective emitter substance for mass spectrometric Pb isotope ratio determinations. Chem. Geol. 136, 309–312.
Gilleaudeau, G.J., Voegelin, A.R., Thibault, N., Moreau, J., Ullmann, C.V., Klaebe, R.M., Korte, C., Frei, R., 2018. Stable isotope records across the Cretaceous-Paleogene transition, Stevns Klint, Denmark: New insights from the chromium isotope system. Geochim. Cosmochim. Acta 235, 305–332.
Goring-Harford, H.J., Klar, J.K., Pearce, C.R., Connelly, D.P., Achterberg, E.P., James, R. H., 2018. Behaviour of chromium isotopes in the eastern sub-tropical Atlantic Oxygen Minimum Zone. Geochim. Cosmochim. Acta 236, 41–59.
Goring-Harford, H.J., Klar, J.K., Donald, H.K., Pearce, C.R., Connelly, D.P., James, R.H., 2020. Behaviour of chromium and chromium isotopes during estuarine mixing in the Beaulieu Estuary, UK. Earth Planet. Sci. Lett. 536, 116166.
Govindaraju, K., 1984. Report (1984) on 2 Git-Iwg Geochemical Reference Samples - Albite from Italy, Al-I and Iron Formation Sample from Greenland, If-G. Geostand. Newslett. 8, 63–113.
Graf, J.L., O'Connor, E.A., van Leeuwen, P., 1994. Rare earth element evidence of origin and depositional environment of late Proterozoic ironstone beds and manganese-oxide deposits, SW Brazil and SE Bolivia. J. South. Earth Sci 7, 115–133.
Guinoiseau, D., Galer, S.J.G., Abouchami, W., Frank, M., Achterberg, E.P., Haug, G.H., 2019. Importance of Cadmium Sulfides for Biogeochemical Cycling of Cd and its Isotopes in Oxygen Deficient Zones—a Case Study of the Angola Basin. Glob. Biogeochem. Cycles 33, 1746–1763.
Gumsley, A.P., Chamberlain, K.R., Bleeker, W., Söderlund, U., de Kock, M.O., Larsson, E. R., Bekker, A., 2017. Timing and tempo of the Great Oxidation Event. Proc. Natl. Acad. Sci. 114, 1811–1816.
Halverson, G.P., Hoffman, P.F., Schrag, D.P., Kaufman, A.J., 2002. A major perturbation of the carbon cycle before the Ghaub glaciation (Neoproterozoic) in Namibia: Prelude to snowball Earth? Geochem. Geophys. Geosyst. 3.
Halverson, G.P., Wade, B.P., Hurtgen, M.T., Barovich, K.M., 2010. Neoproterozoic chemostratigraphy. Precambrian Res. 182, 337–350.
Halverson, G.P., Poitrasson, F., Hoffman, P.F., Nédélec, A., Montel, J.-M., Kirby, J., 2011. Fe isotope and trace element geochemistry of the Neoproterozoic syn-glacial Rapitan iron formation. Earth Planet. Sci. Lett. 309, 100–112.
He, X., Chen, G., Fang, Z., Liang, W., Li, B., Tang, J., Sun, Y., Qin, L., 2020. Source identification of chromium in the sediments of the Xiaoqing River and Laizhou Bay: a chromium stable isotope perspective. Environ. Pollut. 264, 114686.
Heinrichs, H., Schulz-Dobrick, B., Wedepohl, K.H., 1980. Terrestrial geochemistry of Cd, Bi, Tl, Pb, Zn and Rb. Geochim. Cosmochim. Acta 44, 1519–1533.

Hiatt, E.E., Pufahl, P.K., Guimarães da Silva, L., 2020. Iron and phosphorus biochemical systems and the Cryogenian-Ediacaran transition, Jacadigo basin, Brazil: Implications for the Neoproterozoic oxygenation event. Precambrian Res. 337, 105533.
Hodgskiss, M.S.W., Sperling, E.A., 2021. A prolonged, two-step oxygenation of Earth's early atmosphere: support from confidence intervals. Geology 50, 158–162.
Hoffman, P.F., 2009. Pan-glacial—a third state in the climate system. Geol. Today 25, 100–107.
Hoffman, P.F., Kaufman, A.J., Halverson, G.P., Schrag, D.P., 1998. A Neoproterozoic Snowball Earth Science 281, 1342–1346.
Hohl, S.V., Galer, S.J.G., Gamper, A., Becker, H., 2017. Cadmium isotope variations in Neoproterozoic carbonates - a tracer of biologic production? Geochem. Perspect. Lett. 3, 32–44.
Holland, H.D., 1984. The Chemical Evolution of the Atmosphere and Oceans. Princeton Univ. Press, New York.
Horner, T.J., Rickaby, R.E.M., Henderson, G.M., 2011. Isotopic fractionation of cadmium into calcite. Earth Planet. Sci. Lett. 312, 243–253.
Hsi, C.K.D., Langmuir, D., 1985. Adsorption of uranyl onto ferric oxyhydroxides - applications of the surface complexation site-binding model. Geochim. Cosmochim. Acta 49, 1931–1941.
Hu, J., Huang, C., Wang, H., 2020. U-Pb zircon geochronology and geochemistry of metavolcanics and associated iron ores of the magnetite-rich BIF deposits in the Western Kunlun orogenic belt: Constraints on the depositional age, origin and tectonic setting. Ore Geol. Rev. 126, 103751.
Huang, Q., Viehmann, S., Walde, D.H.G., Li, W., 2021. Iron isotope constraints on the metal source and depositional environment of the Neoproterozoic banded iron- and manganese deposits in Urucum, Brazil. Geochemistry 81, 125771.
Imai, N., Terashima, S., Itoh, S., Ando, A., 1996. 1996 compilation of analytical data on nine GSJ geochemical reference samples, "Sedimentary rock series". Geostand. Newslett. 20, 165–216.
Janssen, D.J., Conway, T.M., John, S.G., Christian, J.R., Kramer, D.I., Pedersen, T.F., Cullen, J.T., 2014. Undocumented water column sink for cadmium in open ocean oxygen-deficient zones. Proc. Natl. Acad. Sci. 111, 6888.
Janssen, D.J., Abouchami, W., Galer, S.J.G., Cullen, J.T., 2017. Fine-scale spatial and interannual cadmium isotope variability in the subarctic Northeast Pacific. Earth Planet. Sci. Lett. 472, 241–252.
Janssen, D.J., Abouchami, W., Galer, S.J.G., Purdon, K.B., Cullen, J.T., 2019. Particulate cadmium stable isotopes in the subarctic Northeast Pacific reveal dynamic Cd cycling and a new isotopically light Cd sink. Earth Planet. Sci. Lett. 515, 67–78.
Janssen, D.J., Rickli, J., Quay, P.D., White, A.E., Nasemann, P., Jaccard, S.L., 2020. Biological Control of Chromium Redox and Stable Isotope Composition in the Surface Ocean. Glob. Biogeochem. Cycles 34 e2019GB006397.
Janssen, D.J., Rickli, J., Wille, M., Sepúlveda Steiner, O., Vogel, H., Dellwig, O., Berg, J. S., Bouffard, D., Lever, M.A., Hassler, C.S., Jaccard, S.L., 2022. Chromium cycling in redox-stratified basins challenges δ53Cr paleoredox proxy applications. Geophys. Res. Lett. 49 e2022GL099154.
John, S.G., Helgoe, J., Townsend, E., 2018. Biogeochemical cycling of Zn and Cd and their stable isotopes in the Eastern Tropical South Pacific. Mar. Chem. 201, 256–262.
Johnston, D.T., Poulton, S.W., Dehler, C., Porter, S., Husson, J., Canfield, D.E., Knoll, A. H., 2010. An emerging picture of Neoproterozoic Ocean chemistry: Insights from the Chuar Group, Grand Canyon, USA. Earth Planet. Sci. Lett. 290, 64–73.
Kämpf, J., Chapman, P., 2016. Upwelling Systems of the World. A Scientific Journey to the Most Productive Marine Ecosystems. Springer Cham, Switzerland.
Kato, Y., Yamaguchi, K.E., Ohmoto, H., 2006. Rare Earth Elements in Precambrian Banded Iron Formations: Secular Changes of Ce and Eu Anomalies and Evolution of Atmospheric Oxygen. In: Kesler, S.E., Ohmoto, H. (Eds.), Evolution of Early Earth's Atmosphere, Hydrosphere, and Biosphere - Constraints from Ore Deposits. Geological Society of America.
Kirschvink, J.L., 1992. Late Proterozoic low-latitude global glaciation: The snowball Earth. In: Schopf, J.W., Klein, c. (Eds.), The Proterozoic Biosphere: A Multidisciplinary Study. Cambridge University Press, Cambridge, pp. 51–53.
Klein, C., 2005. Some Precambrian banded iron-formations (BIFs) from around the world: their age, geologic setting, mineralogy, metamorphism, geochemistry, and origin. Am. Mineral. 90, 1473–1499.
Klein, C., Beukes, N.J., 1993. Sedimentology and Geochemistry of the Glaciogenic late Proterozoic Rapitan Iron-Formation in Canada. Econ. Geol. 88, 542–565.
Klein, C., Ladeira, E.A., 2004. Geochemistry and mineralogy of neoproterozoic banded iron-formations and some selected, siliceous manganese formations from the Urucum district, Mato Grosso do Sul, Brazil. Econ. Geol. 99, 1233–1244.
Konhauser, K.O., Lalonde, S.V., Planavsky, N.J., Pecoits, E., Lyons, T.W., Mojzsis, S.J., Rouxel, O.J., Barley, M.E., Rosiere, C., Fralick, P.W., Kump, L.R., Bekker, A., 2011. Aerobic bacterial pyrite oxidation and acid rock drainage during the Great Oxidation Event. Nature 478, 369–373.
Krause, A.J., Mills, B.J.W., Merdith, A.S., Lenton, T.M., Poulton, S.W., 2022. Extreme variability in atmospheric oxygen levels in the late Precambrian. Science. Advances 8, eabm8191.
Lambelet, M., Rehkamper, M., de Flierdt, T.V., Xue, Z.C., Kreissig, K., Coles, B., Porcelli, D., Andersson, P., 2013. Isotopic analysis of Cd in the mixing zone of Siberian rivers with the Arctic Ocean-New constraints on marine Cd cycling and the isotope composition of riverine Cd. Earth Planet. Sci. Lett. 361, 64–73.
Le Hir, G., Donnadieu, Y., Godderis, Y., Pierrehumbert, R.T., Halverson, G.R., Macouin, M., Nedelec, A., Ramstein, G., 2009. The snowball Earth aftermath: Exploring the limits of continental weathering processes. Earth Planet. Sci. Lett. 277, 453–463.
Li, C., Love, G.D., Lyons, T.W., Fike, D.A., Sessions, A.L., Chu, X.L., 2010. A stratified redox model for the Ediacaran Ocean. Science 328, 80–83.
Li, Z.-Q., Zhang, L.-C., Xue, C.-J., Zheng, M.-T., Zhu, M.-T., Robbins, L.J., Slack, J.F., Planavsky, N.J., Konhauser, K.O., 2018. Earth's youngest banded iron formation implies ferruginous conditions in the early Cambrian Ocean. Sci. Rep. 8, 9970.
Liang, M.C., Hartman, H., Kopp, R.E., Kirschvink, J.L., Yung, Y.L., 2006. Production of hydrogen peroxide in the atmosphere of a Snowball Earth and the origin of oxygenic photosynthesis. Proc. Natl. Acad. Sci. USA 103, 18896–18899.
Liger, E., Charlet, L., Van Cappellen, P., 1999. Surface catalysis of uranium(VI) reduction by iron(II). Geochim. Cosmochim. Acta 63, 2939–2955.
Little, S.H., Vance, D., Lyons, T.W., McManus, J., 2015. Controls on trace metal authigenic enrichment in reducing sediments: Insights from modern oxygen-deficient settings. Am. J. Sci. 315, 77–119.
Liu, J., Zhu, R., Ma, L., Fu, H., Lin, X., Parker, S.C., Molinari, M., 2021. Adsorption of phosphate and cadmium on iron (oxyhydr)oxides: a comparative study on ferrihydrite, goethite, and hematite. Geoderma 383, 114799.
Lyons, T.W., Werne, J.P., Hollander, D.J., Murray, R.W., 2003. Contrasting sulfur geochemsitry and Fe/Al and Mo/al ratios across the last oxic-to-anoxic transition in the Cariaco Basin, Venezuela. Chem. Geol. 195, 131–157.
Matheson, E.J., Pufahl, P.K., Voinot, A., Murphy, J.B., Fitzgerald, D.M., 2022. Ironstone as a proxy of Paleozoic Ocean oxygenation. Earth Planet. Sci. Lett. 594, 117715.
McDonough, W.F., Sun, S.-S., 1995. The composition of the Earth. Chem. Geol. 120, 223–253.
McLennan, S.M., 1989. Rare earth elements in sedimentary rocks; influence of provenance and sedimentary processes. Rev. Mineral. Geochem. 21, 169–200.
Moczydlowska, M., 2008. The Ediacaran microbiota and the survival of Snowball Earth conditions. Precambrian Res. 167, 1–15.
Morais, L., Freitas, B.T., Fairchild, T.R., Toniolo, T.F., Campos, M.D.R., Prado, G.M.E.M., Silva, P.A.S., Rudnitzki, I.D., Lahr, D.J.G., Leme, J.M., Philippot, P., Lopez, M., Trindade, R.I.F., 2021. Diverse vase-shaped microfossils within a Cryogenian glacial setting in the Urucum Formation (Brazil). Precambrian Res. 367, 106470.
Morford, J.L., Emerson, S., 1999. The geochemistry of redox sensitive trace metals in sediments. Geochim. Cosmochim. Acta 63, 1735–1750.
Narbonne, G.M., 2005. The ediacarabiota: Neoproterozoic origin of animals and their ecosystems. Annu. Rev. Earth Planet. Sci. 33, 421–442.
Novak, M., Kram, P., Sebek, O., Andronikov, A., Chrastny, V., Martinkova, E., Stepanova, M., Prechova, E., Curik, J., Veselovsky, F., Myska, O., Stedra, V., Farkas, J., 2017. Temporal changes in Cr fluxes and δ53Cr values in runoff from a small serpentinite catchment (Slavkov Forest, Czech Republic). Chem. Geol. 472, 22–30.
Nozaki, Y., Zhang, J., Amakawa, H., 1997. The fractionation between Y and Ho in the marine environment. Earth Planet. Sci. Lett. 148, 329–340.
Oze, C., Bird, D.K., Fendorf, S., 2007. Genesis of hexavalent chromium from natural sources in soil and groundwater. Proc. Natl. Acad. Sci. 104, 6544–6549.
Partin, C.A., Lalonde, S.V., Planavsky, N.J., Bekker, A., Rouxel, O.J., Lyons, T.W., Konhauser, K.O., 2013. Uranium in iron formations and the rise of atmospheric oxygen. Chem. Geol. 362, 82–90.
Paulukat, C., Dossing, L.N., Mondal, S.K., Voegelin, A.R., Frei, R., 2015. Oxidative release of chromium from Archean ultramafic rocks, its transport and environmental impact - a Cr isotope perspective on the Sukinda valley ore district (Orissa, India). Appl. Geochem. 59, 125–138.
Paulukat, C., Gilleaudeau, G.J., Chernyavskiy, P., Frei, R., 2016. The Cr-isotope signature of surface seawater - a global perspective. Chem. Geol. 444, 101–109.
Peltier, W.R., Liu, Y.G., Crowley, J.W., 2007. Snowball Earth prevention by dissolved organic carbon remineralization. Nature 450, 813–U811.
Pereira, N.S., Voegelin, A.R., Paulukat, C., Sial, A.N., Ferreira, V.P., Frei, R., 2015. Chromium-isotope signatures in scleractinian corals from the Rocas Atoll, Tropical South Atlantic. Geobiology 14, 54–67.
Petersen, W., Wallmann, K., Schröer, S., Schroeder, F., 1993. Studies on the adsorption of cadmium on hydrous iron(III) oxides in oxic sediments. Anal. Chim. Acta 273, 323–327.
Piacentini, T., Boggiani, P.C., Yamamoto, J.K., Freitas, B.T., da Cruz Campanha, G.A., 2007. Formação ferrífera associada à sedimentação glaciogênica da Formação Puga (Marinoano) na Serra da Bodoquena, MS. Revista Brasileira de Geociências 37, 530–541.
Piacentini, T., Vasconcelos, P.M., Farley, K.A., 2013. Ar-40/Ar-39 constraints on the age and thermal history of the Urucum Neoproterozoic banded iron-formation, Brazil. Precambrian Res. 228, 48–62.
Plass, A., Schlosser, C., Sommer, S., Dale, A.W., Achterberg, E.P., Scholz, F., 2020. The control of hydrogen sulfide on benthic iron and cadmium fluxes in the oxygen minimum zone off Peru. Biogeosciences 17, 3685–3704.
Polgári, M., Biondi, J.C., Gyollai, I., Fintor, K., Szabó, M., 2021. Origin of the Urucum iron formations (Neoproterozoic, Brazil): Textural and mineralogical evidence (Mato Grosso do Sul – Brazil). Ore Geol. Rev. 139, 104456.
Poulton, S.W., Fralick, P.W., Canfield, D.E., 2010. Spatial variability in oceanic redox structure 1.8 billion years ago. Nat. Geosci. 3, 486–490.
Poulton, S.W., Bekker, A., Cumming, V.M., Zerkle, A.L., Canfield, D.E., Johnston, D.T., 2021. A 200-million-year delay in permanent atmospheric oxygenation. Nature 592, 232–236.
Randall, S.R., Sherman, D.M., Ragnarsdottir, K.V., Collins, C.R., 1999. The mechanism of cadmium surface complexation on iron oxyhydroxide minerals. Geochim. Cosmochim. Acta 63, 2971–2987.
Rehkämper, M., Wombacher, F., Horner, T.J., Xue, Z., 2012. Natural and Anthropogenic Cd Isotope Variations. In: Baskaran, M. (Ed.), Handbook of Environmental Isotope Geochemistry, vol. I. Springer Berlin Heidelberg, Berlin, Heidelberg, pp. 125–154.
Rickli, J., Janssen, D.J., Hassler, C., Ellwood, M.J., Jaccard, S.L., 2019. Chromium biogeochemistry and stable isotope distribution in the Southern Ocean. Geochim. Cosmochim. Acta 262, 188–206.

Ripperger, S., Rehkamper, M., 2007. Precise determination of cadmium isotope fractionation in seawater by double spike MC-ICPMS. Geochim. Cosmochim. Acta 71, 631–642.
Ripperger, S., Rehkamper, M., Porcelli, D., Halliday, A.N., 2007. Cadmium isotope fractionation in seawater - a signature of biological activity. Earth Planet. Sci. Lett. 261, 670–684.
Rosenthal, Y., Boyle, E.A., Labeyrie, L., Oppo, D., 1995a. Glacial enrichments of authigenic Cd and U in subantarctic sediments: a climatic control on the elements' oceanic budget? Paleoceanography 10, 395–413.
Rosenthal, Y., Lam, P., Boyle, E.A., Thomson, J., 1995b. Authigenic cadmium enrichments in suboxic sediments: Precipitation and postdepositional mobility. Earth Planet. Sci. Lett. 132, 99–111.
Rudge, J.F., Reynolds, B.C., Bourdon, B., 2009. The double spike toolbox. Chem. Geol. 265, 420–431.
Scheiderich, K., Amini, M., Holmden, C., Francois, R., 2015. Global variability of chromium isotopes in seawater demonstrated by Pacific, Atlantic, and Arctic Ocean samples. Earth Planet. Sci. Lett. 423, 87–97.
Schier, K., Bau, M., Smith, A.J.B., Beukes, N.J., Coetzee, L.L., Viehmann, S., 2020. Chemical evolution of seawater in the Transvaal Ocean between 2426 Ma (Ongeluk large Igneous Province) and 2413 Ma ago (Kalahari Manganese Field). Gondwana Res. 88, 373–388.
Schmitt, A.D., Galer, S.J.G., Abouchami, W., 2009. Mass-dependent cadmium isotopic variations in nature with emphasis on the marine environment. Earth Planet. Sci. Lett. 277, 262–272.
Schoenberg, R., Zink, S., Staubwasser, M., von Blanckenburg, F., 2008. The stable Cr isotope inventory of solid Earth reservoirs determined by double spike MC-ICP-MS. Chem. Geol. 249, 294–306.
Semeniuk, D.M., Maldonado, M.T., Jaccard, S.L., 2016. Chromium uptake and adsorption in marine phytoplankton - Implications for the marine chromium cycle. Geochim. Cosmochim. Acta 184, 41–54.
Sial, A.N., Campos, M.S., Gaucher, C., Frei, R., Ferreira, V.P., Nascimento, R.C., Pimentel, M.M., Pereira, N.S., Rodler, A., 2015. Algoma-type Neoproterozoic BIFs and related marbles in the Seridó Belt (NE Brazil): REE, C, O, Cr and Sr isotope evidence. J. South. Earth Sci. 61, 33–52.
Sieber, M., Conway, T.M., de Souza, G.F., Obata, H., Takano, S., Sohrin, Y., Vance, D., 2019. Physical and biogeochemical controls on the distribution of dissolved cadmium and its isotopes in the Southwest Pacific Ocean. Chem. Geol. 511, 494–509.
Slack, J.F., Grenne, T., Bekker, A., Rouxel, O.J., Lindberg, P.A., 2007. Suboxic deep seawater in the late Paleoproterozoic: evidence from hematitic chert and iron formation related to seafloor-hydrothermal sulfide deposits, Central Arizona, USA. Earth Planet. Sci. Lett. 255, 243–256.
Stern, R.J., Mukherjee, S.K., Miller, N.R., Ali, K., Johnson, P.R., 2013. ~750Ma banded iron formation from the Arabian-Nubian Shield—Implications for understanding neoproterozoic tectonics, volcanism, and climate change. Precambrian Res. 239, 79–94.
Swanson-Hysell, N.L., Rose, C.V., Calmet, C.C., Halverson, G.P., Hurtgen, M.T., Maloof, A.C., 2010. Cryogenian Glaciation and the Onset of Carbon-Isotope Decoupling. Science 328, 608–611.
Sweere, T.C., Dickson, A.J., Jenkyns, H.C., Porcelli, D., Ruhl, M., Murphy, M.J., Idiz, E., van den Boorn, S.H.J.M., Eldrett, J.S., Henderson, G.M., 2020. Controls on the Cd-isotope composition of Upper cretaceous (Cenomanian–Turonian) organic-rich mudrocks from South Texas (Eagle Ford Group). Geochim. Cosmochim. Acta 287, 251–262.
Tachikawa, K., Handel, C., Dupré, B., 1997. Distribution of rare earth elements and neodymium isotopes in settling particulate material of the tropical Atlantic Ocean (EUMELI site). Deep-Sea Res. I Oceanogr. Res. Pap. 44, 1769–1792.
Taylor, S.R., McLennan, S.M., 1985. The Continental Crust: Its Composition and Evolution. Blackwell, Oxford.
Trinquier, A., Birck, J.L., Allegre, C.J., 2008. High-precision analysis of chromium isotopes in terrestrial and meteorite samples by thermal ionization mass spectrometry. J. Anal. At. Spectrom. 23, 1565–1574.
Trompette, R., De Alvarenga, C.J.S., Walde, D., 1998. Geological evolution of the Neoproterozoic Corumba graben system (Brazil). Depositional context of the stratified Fe and Mn ores of the Jacadigo group. J. South. Earth Sci. 11, 587–597.
Urban, H., Stribrny, B., Lippolt, H.J., 1992. Iron and manganee deposits of the Urucum district, Mato-Grosse-do-Sul, Brazil. Econ. Geol. 87, 1375–1392.
van Geen, A., McCorkle, D.C., Klinkhammer, G.P., 1995. Sensitivity of the phosphate-cadmium-carbon isotope relation in the ocean to cadmium removal by suboxic sediments. Paleoceanography 10, 159–169.
Viehmann, S., Bau, M., Bühn, B., Dantas, E.L., Andrade, F.R.D., Walde, D.H.G., 2016. Geochemical characterisation of Neoproterozoic marine habitats: evidence from trace elements and Nd isotopes in the Urucum iron and manganese formations, Brazil. Precambrian Res. 282, 74–96.
Walde, D.H.G., Hagemann, S.G., 2007. The Neoproterozoic Urucum/Mutun Fe and Mn deposits in W-Brazil/SE-Bolivia: assessment of ore deposit models. Zeitschrift Der Deutschen Gesellschaft Fur Geowissenschaften 158, 45–55.
Walde, D.H.G., do Carmo, D.A., Guimaraes, E.M., Vieira, L.C., Erdtmann, B.D., Sanchez, E.A.M., Adorno, R.R., Tobias, T.C., 2015. New aspects of Neoproterozoic-Cambrian transition in the Corumba region (state of Mato Grosso do Sul, Brazil). Ann. Paleontol. 101, 213–224.
Wang, X.L., Planavsky, N.J., Hull, P.M., Tripati, A.E., Zou, H.J., Elder, L., Henehan, M., 2016. Chromium isotopic composition of core-top planktonic foraminifera. Geobiology 15, 51–64.
Wang, X., Jing, Y., Peng, H., Yang, H., Zhu, Z., Chen, Z.-Q., 2023. Cadmium isotope evidence deciphers enhanced marine productivity during the middle Mesoproterozoic (the Xiamaling formation, North China). Precambrian Res. 389, 107021.
Wasylenki, L.E., Swihart, J.W., Romaniello, S.J., 2014. Cadmium isotope fractionation during adsorption to Mn oxyhydroxide at low and high ionic strength. Geochim. Cosmochim. Acta 140, 212–226.
Wei, W., Frei, R., Chen, T.-Y., Klaebe, R., Liu, H., Li, D., Wei, G.-Y., Ling, H.-F., 2018a. Marine ferromanganese oxide: a potentially important sink of light chromium isotopes? Chem. Geol. 495, 90–103.
Wei, W., Frei, R., Gilleaudeau, G.J., Li, D., Wei, G.-Y., Chen, C., Ling, H.-F., 2018b. Oxygenation variations in the atmosphere and shallow seawaters of the Yangtze Platform during the Ediacaran Period: Clues from Cr-isotope and Ce-anomaly in carbonates. Precambrian Res. 313, 78–90.
Wei, W., Frei, R., Klaebe, R., Li, D., Wei, G.-Y., Ling, H.-F., 2018c. Redox condition in the Nanhua Basin during the waning of the Sturtian glaciation: a chromium-isotope perspective. Precambrian Res. 319, 198–210.
Wu, W., Wang, X., Reinhard, C.T., Planavsky, N.J., 2017. Chromium isotope systematics in the Connecticut River. Chem. Geol. 456, 98–111.
Xie, R.C., Galer, S.J.G., Abouchami, W., Rijkenberg, M.J.A., de Baar, H.J.W., De Jong, J., Andreae, M.O., 2017. Non-Rayleigh control of upper-ocean Cd isotope fractionation in the western South Atlantic. Earth Planet. Sci. Lett. 471, 94–103.
Xue, Z.C., Rehkamper, M., Horner, T.J., Abouchami, W., Middag, R., van de Flierdt, T., de Baar, H.J.W., 2013. Cadmium isotope variations in the Southern Ocean. Earth Planet. Sci. Lett. 382, 161–172.
Yan, X., Zhu, M., Li, W., Peacock, C.L., Ma, J., Wen, H., Liu, F., Zhou, Z., Zhu, C., Yin, H., 2021. Cadmium Isotope Fractionation during Adsorption and Substitution with Iron (Oxyhydr)oxides. Environ. Sci. Technol. 55, 11601–11611.
Yang, S.-C., Lee, D.-C., Ho, T.-Y., Wen, L.-S., Yang, H.-H., 2014. The isotopic composition of dissolved cadmium in the water column of the West Philippine Sea. Frontiers in Marine. Science 1.
Yin, J., Li, H., Xiao, K., 2023. Origin of Banded Iron Formations: Links with Paleoclimate, Paleoenvironment, and Major Geological Processes, (Minerals).
Yu, L., Chen, W., Zhang, B., Tian, L., Liu, S., Yang, D., Wang, L., 2022. The genesis of the early Neoproterozoic Shilu banded iron formations: could it be applied to other iron ore deposits? Ore Geol. Rev. 140, 104424.